Progress in Oceanography 173 (2019) 238–255

Contents lists available at ScienceDirect

Progress in Oceanography

journal homepage: www.elsevier.com/locate/pocean

Seasonal modulation of mesoscale processes alters nutrient availability and plankton communities in the Red Sea

Benjamin Kürten[a,*], Nikolaos D. Zarokanellos[a,b,1], Reny P. Devassy[c], Mohsen M. El-Sherbiny[c,d,2], Ulrich Struck[e,f], Douglas G. Capone[g], Isabelle K. Schulz[a], Ali M. Al-Aidaroos[c], Xabier Irigoien[a,h,3], Burton H. Jones[a]

[a] King Abdullah University of Science and Technology (KAUST), Red Sea Research Center (RSRC), Biological and Environmental Sciences & Engineering Division (BESE), Thuwal 23955-6900, Saudi Arabia
[b] Balearic Islands Coastal Observing and Forecasting System (SOCIB), ParcBit, Edif. Naorte, 07121 Palma de Mallorca, Spain
[c] King Abdulaziz University, Department of Marine Biology, Faculty of Marine Sciences, P.O. Box 80207, Jeddah 21589, Saudi Arabia
[d] Suez Canal University, Department of Marine Science, Faculty of Science, 41522 Ismailia, Egypt
[e] Leibniz Institute for Research on Evolution and Biodiversity, Museum of Natural History, Invalidenstraße 43, 10115 Berlin, Germany
[f] Freie Universität Berlin, Department of Earth Sciences, Malteserstraße 74-100, 12249 Berlin, Germany
[g] University of Southern California, Department of Biological Sciences & Wrigley Institute for Environmental Studies, 3616 Trousdale Parkway, Los Angeles, CA 90089-0371, United States
[h] AZTI-Tecnalia, Herrera Kaia, 20110 Pasaia, Spain

ARTICLE INFO

Keywords:
Biogeochemistry
Circulation
Diatom-Diazotroph Associations (DDAs)
Mesoscale eddies
Seawater oxygen stable isotopes ($\delta^{18}O_{SW}$)
Trichodesmium
Red Sea

ABSTRACT

Hydrographic and atmospheric forcing set fundamental constraints on the biogeochemistry of aquatic ecosystems and manifest in the patterns of nutrient availability and recycling, species composition of communities, trophic dynamics, and ecosystem metabolism. In the Red Sea, latitudinal gradients in environmental conditions and primary production have been ascribed to fluctuations in Gulf of Aden Water inflow, upwelling/mixing, and regenerated nutrient utilization i.e. rapidly recycled nitrogen in upper layers. However, our understanding of upper layer dynamics and related changes in plankton communities, metabolism and carbon and nitrogen export is limited. We surmised that stratification and mesoscale eddies modulate the nutrient availability and taxonomic identity of plankton communities in the Red Sea. Based on remote-sensing data of sea level anomalies and high resolution in situ measurements (ScanFish) we selected stations for hydrographic CTD profiles, water sampling (nutrients, seawater oxygen stable isotopes [$\delta^{18}O_{SW}$]), phytoplankton and zooplankton collections. In fall 2014, strong stratification subjected the plankton community to an overall nitrogen and phosphorus shortage. The nutrient deficiency increased numbers of heterotrophic dinoflagellates, microzooplankton, and diazotrophs (*Trichodesmium*, diatom-diazotroph associations [DDAs]), albeit largely decreased phytoplankton and mesozooplankton abundances. In spring 2015, mesoscale eddies increased the nutrient availability, and the thermohaline characteristics and low $\delta^{18}O_{SW}$ point to the interaction of eddies with Gulf of Aden Surface Water (GASW). Cyclonic eddies and, most likely, the availability of nutrients associated with the GASW, increased the abundances of autotrophs (diatoms, Prasinophytes) and supported larger numbers of zooplankton and their larvae. We demonstrate that the interplay of stratification, advection of Gulf of Aden water and mesoscale eddies are key elements to better understand changes in plankton community composition, ecosystem metabolism, and macronutrient export in the Red Sea in space and time.

1. Introduction

The Red Sea is a canonical prototype of epicontinental seas, where fundamental physical and biogeochemical processes can be studied in relation to climatological conditions at a basin-wide scale. The Red Sea is a marginal sea of the Indian Ocean and a geologically young oceanic

* Corresponding author.
E-mail address: kuertenb@gmail.com (B. Kürten).
[1] Present address: Balearic Islands Coastal Observing and Forecasting System (SOCIB), ParcBit, Edif. Naorte, 07121 Palma, Spain.
[2] Present address: King Abdulaziz University, Department of Marine Biology, Faculty of Marine Sciences, P.O. Box 80207, Jeddah 21589, Saudi Arabia.
[3] Present address: AZTI-Tecnalia, Herrera Kaia, 20110 Pasaia, Spain.

https://doi.org/10.1016/j.pocean.2019.02.007
Received 29 May 2017; Received in revised form 15 January 2019; Accepted 7 February 2019
Available online 08 February 2019
0079-6611/ © 2019 The Authors. Published by Elsevier Ltd. This is an open access article under the CC BY-NC-ND license (http://creativecommons.org/licenses/BY-NC-ND/4.0/).

analog of the Atlantic Ocean ~100 Mya (Litvin, 1984; Brathwaite, 1987). Atmospheric and thermohaline forces drive the circulation of the Red Sea (Quadfasel and Baudner, 1993). Resembling the Atlantic Meridional Overturning Circulation (AMOC), high evaporation and cooling in the Red Sea induce a reverse-estuarine circulation (Neumann and McGill, 1962; Abualnaja et al., 2015). Latitudinal gradients of environmental conditions and plankton biogeography have been ascribed to the water exchange with the Indian Ocean through the Strait of Bab-al-Mandab and subsequent changes in physical and chemical properties within the basin (Grasshoff, 1969; Halim, 1969; Siccha et al., 2009). The Indian Ocean monsoon influences the circulation of the Red Sea by reversing the prevailing wind direction over the southern half of the Red Sea (south of ~20°N) and regulating the exchange of water with the Gulf of Aden and the Indian Ocean (Barlow, 1934; Sverdrup et al., 1942; Morcos, 1970; Patzert, 1974; Johns and Sofianos, 2012).

Two distinct water masses from the Gulf of Aden are distinguishable based on their physical and biochemical characteristics in the Red Sea. The exchange flow with the Gulf of Aden chiefly alternates between the inflow of Gulf of Aden Surface Water (GASW) in winter (Indian NE monsoon) and Gulf of Aden Intermediate Water (GAIW) in summer (Indian SW monsoon) (Patzert, 1974; Sofianos et al., 2002; Sofianos and Johns, 2007). GASW is a warmer (> 29.8 °C) surface inflow, whereas GAIW enters as a relatively colder intrusion at intermediate depths and centers between the 26–26.5 kg m^{-3} isopycnals in the central Red Sea (Sofianos et al., 2002; Zarokanellos et al., 2017a). The intrusion of GASW typically begins in early September and lasts until the end of March (Barlow, 1934; Sofianos et al., 2002). The inflow of GASW is more homogenous and more voluminous than the inflow of GAIW because it compensates for the more substantial evaporative loss in winter (Murray and Johns, 1997; Sofianos et al., 2002). The GASW surface flow sets north-northwest (into the Red Sea) where its path and physicochemical properties are influenced by cyclonic and anticyclonic mesoscale structures (Grasshoff, 1969; Zhan et al., 2014; Zarokanellos et al., 2017b; Zarokanellos and Jones, 2018). The GAIW intrusion lasts approximately from summer to late fall (Murray and Johns, 1997), and advects northwards with speeds as much as 30–65 cm s^{-1} (Siedler, 1968; Jones and Browning, 1971; Churchill et al., 2014). The GAIW forms an eastern boundary current north of 16°N and a reverse southbound flow along the northwestern coast (Barlow, 1934; Churchill et al., 2014; Bower and Farrar, 2015).

The central Red Sea (20–25°N) is the most oligotrophic area and lies between the mostly little productive northern (25–28°N) and the more productive southern Red Sea (14–20°N; Halim, 1969; Raitsos et al., 2013). In situ observations and remote-sensing studies characterized the central Red Sea as an area with dynamic mesoscale activity and quasi-persistent anticyclonic eddies even though cyclonic structures are present (Quadfasel and Baudner, 1993; Sofianos and Johns, 2002; Raitsos et al., 2013; Chen et al., 2014). In fact, the transports in the upper layer associated with these eddies are more voluminous compared to the mean along axis flow (Quadfasel and Baudner, 1993). In addition to their influence on the upper-layer circulation, recurrent mesoscale eddy activity in the Red Sea may be the key to understand the distribution of plankton and biogeochemical processes.

Mesoscale eddy activity has long been recognized as a fundamental physical-biogeochemical interaction (McGillicuddy, 2016). Recent numerical simulations (Zhan et al., 2014) and in situ observations (Kürten et al., 2016; Qurban et al., 2017; Zarokanellos et al., 2017a; Zarokanellos and Jones, 2018) indicated high but variable cyclonic and anticyclonic mesoscale eddy activity in the central Red Sea. The uplifting of the pycnoclines by mesoscale structures alters the vertical density-nutrients gradient by enhancing nutrient concentrations in the euphotic layer. Such episodic disturbances in the physical environment typically result in changes in the communities of primary producers, because eddies alter the accessibility and relative (stoichiometric) proportions of nutrients, such as nitrogen (N), phosphorus (P) and silicate (Si), and modulate the succession and competition of phytoplankton as well as the planktonic food web architecture (Legendre and Rassoulzadegan, 1995; Sommer et al., 2002b; Sterner and Elser, 2002).

In oligotrophic oceans, injections of nutrients often promote the temporary growth of fast-growing diatoms (Goldman, 1988), while mixo-/heterotrophic dinoflagellates and smaller zooplankton prevail when nutrients are deficient (Officer and Ryther, 1980; Egge and Aksnes, 1992; Bibby and Moore, 2011). Building on this divergence in food web architecture, proportional abundances of diatoms and mixo-/heterotrophic dinoflagellates were used to indicate ecosystem health, the flow of energy through food webs, and export at geological time scales (Sommer et al., 2002b; Seeberg-Elverfeldt et al., 2005; Wasmund, 2017). Thus, knowledge about the (relative) abundances of diatoms and dinoflagellates in the Red Sea is particularly informative of upper layer processes as productivity occurs primarily at the deep chlorophyll maximum (DCM) (Weikert, 1987), and seasonality in the annual deposition cycle is strong (Seeberg-Elverfeldt et al., 2005).

The oligotrophy in the upper layers of the Red Sea has been ascribed to negligible nutrient input via precipitation and terrestrial run-off (Morcos, 1970), and stratification (Yao et al., 2014). In the northern Red Sea, where nutrients are scarce, phytoplankton communities are dominated by ultraphytoplankton, whereas larger taxa such as diatoms are more abundant in the southern Red Sea (Halim, 1969; Kürten et al., 2016; Pearman et al., 2016a). This North–South gradient in plankton composition and productivity is primarily attributable to the inflow of GAW, although diatoms and herbivorous zooplankton periodically thrive also in the central and northern Red Sea in response to upwelling and deep mixing (Lindell and Post, 1995; Dreano et al., 2016; Kürten et al., 2016; Pearman et al., 2016a; Kheiredine et al., 2017). The GAIW is relatively rich in nutrients (dissolved inorganic nitrogen > 14 μM) and chromophoric dissolved organic matter (CDOM > 1.5 ppb) (Churchill et al., 2014; Zarokanellos et al., 2017a), and transports large quantities of plankton into the Red Sea (Halim, 1969). However, many plankton organisms die-off upon import into the Red Sea as the salinity increases (Weikert, 1987), and their decomposition likely contributes to the dissolved nutrient pool of the GAW (Beckmann, 1984).

Diazotrophs play a substantial role in the nutrient cycles of the Red Sea (Naqvi et al., 1986), even though their trophodynamic relevance decreases from North to South (Kürten et al., 2014, 2016). The capacity of dinitrogen (N_2) fixation offers diazotrophic plankton an ecological advantage during periods of reduced N availability. Information about the spatial distribution of N_2 fixation rates in the Red Sea and the diazotrophic species involved are limited compared to many other regions of the global oceans (Sohm et al., 2011b). Quantitatively substantial N_2 fixation in the Red Sea has been ascribed to the cyanobacterium *Trichodesmium erythraeum* (hereafter *Trichodesmium*) (Ehrenberg, 1830; Naqvi et al., 1986; Böttger-Schnack and Schnack, 1989; Foster et al., 2009; Kürten et al., 2015). Also diatom-diazotroph associations (DDAs) of the diatom genera *Rhizosolenia* and *Hemiaulus* with the cyanobacterium *Richelia intracellularis* occur frequently in the Red Sea (Kimor et al., 1992; Kürten et al., 2015) and contribute to the nutrient cycling in the Red Sea.

Seawater oxygen stable isotopes ($\delta^{18}O_{SW}$, ‰) constitute a conservative geochemical tracer of water masses (Craig and Gordon, 1965). The latitudinal $\delta^{18}O_{SW}$ gradient in the surface waters of the Red Sea, ranging from ~0.8‰ in the Strait of Bab-al-Mandab in the South to values of more than 2‰ in the North, is closely associated with increasing salinity (Craig, 1966; Andrié and Merlivat, 1989). As Gulf of Aden Water (GAW) meanders northward in the Red Sea, its thermohaline characteristics are altered by evaporation and cooling at the surface so that its density increases, whilst effects of precipitation and river runoff can be disregarded in the $\delta^{18}O_{SW}$ budget. In combination with salinity data, $\delta^{18}O_{SW}$ conveys information about physical processes (i.e. evaporation/precipitation and upwelling/advection) that are independent of biological nutrient dynamics (Rohling and Bigg, 1998; McGuire and McDonnell, 2007; Bigg and Rohling, 2000).

Accordingly, intrusions of GAW and residence time of water in the Red Sea can be estimated from $\delta^{18}O$ in foraminifera (e.g., Ganssen and Kroon, 1991; Hemleben et al., 1996).

The ecological implications of mesoscale features on the taxonomic identity of plankton communities and their productivity in the Red Sea have received little attention. Based on an extensive data set of carbon and nitrogen isotopes of plankton, Kürten et al. (2016) conceptualized the primary sources of nutrients for plankton communities in the Red Sea in an ecohydrographic framework. These sources include (1) upwelling/deep mixing (Lindell and Post, 1995; Kürten et al., 2016), (2) diazotrophy (Naqvi et al., 1986; Souvermezoglou et al., 1989), (3) GAIW (Churchill et al., 2014), and (4) aeolian dust deposits (Wedyan et al., 2007; Wankel et al., 2010; Li et al., 2018). However, sustained controversy continued as to which physical processes govern pelagic trophodynamics, the balance between new and regeneration production, and macronutrient export/sequestration.

The objective of the present study was to provide an integrated description of the interplay between oceanographic processes and the associated modulation of the nutrient availability for plankton communities in the central Red Sea. Changing biogeochemistry affects trophic interactions and ecosystem processes by altering the elemental ratios of key plankton species and assemblages, the transfer of C, N, and P through biotic and abiotic nutrient pools, and the ecosystem metabolism (Welti et al., 2017). As the significance of the potential sources of nutrients varies in time and space, it was hypothesized that the intrusion of water from the Gulf of Aden and mesoscale eddy structures hold the primary key to understand the ecohydrography of the Red Sea. Using microscope count data and complementary pigment-based fingerprinting approaches, we describe how stratification and eddies alter the microphytoplankton and zooplankton communities in fall 2014 and spring 2015. We document the presence of GAW in the central Red Sea based on temperature-salinity relationships and low $\delta^{18}O_{SW}$. Subsequently, we discuss the implications of upper layer dynamics for the ecosystem metabolism in the Red Sea.

2. Materials and method

2.1. Adaptive cruise outline

For the '*Nutrient Cycling in the Red Sea*' (NC) project, surveys were conducted in fall 2014 and spring 2015 aboard R/V *Thuwal* in the central Red Sea (Fig. 1; Table 1). Remotely-sensed Sea Level Anomalies (SLA) data (http://marine.copernicus.eu, SEALEVEL_GLO_SLA_MAP_L4_REP_OBSERVATIONS_008_027) and Sea Surface Temperatures (SST) (https://oceandata.sci.gsfc.nasa.gov, HMODISA Level-3 Standard Mapped Image SST data) were considered for the cruise planning (Fig. 1B and C). During both cruises, SSTs were within the range of SSTs typical for the period of 2002–2017 in the central Red Sea (Supplementary Fig. 1).

In the fall, the positioning of the stations along the cruise track was based on remotely-sensed information of SLA (Fig. 1B). In spring, we first carried out an uninterrupted (Leg 1: 30 March–2 April; 45.5 h) towed vehicle survey (ScanFish II, EIVA a/s, DK) from 24.2 to 19.7°N (Fig. 1C). The ScanFish track followed a slightly adjusted cruise trajectory to that used in fall 2014 and considered latest SLA data. The ScanFish was equipped with a CTD (SBE 9+, Sea-Bird), a fluorescence and an oxygen sensor (FLBTURB, SBE 43, respectively; Sea-Bird). Undulating from 5 to 160 m and towed at a speed of ~7 knots, dive cycles of 10 min provided a horizontal resolution of ~2.1 km at mid-depth. Data from each cycle were averaged into individual vertical profiles, and gridded with an horizontal and vertical spacing of 2 km and 1 m, respectively. Time-stamps were checked for monotony, and GPS-positions were visually validated and interpolated where necessary.

2.2. Field sampling

Locations for conductivity, temperature, depth (CTD) profiling and water sample collections (Leg 2: 3–9 April 2015) were adapted on the basis of oceanographic features observed during the ScanFish survey (Fig. 1C). Vertical CTD and dissolved oxygen profiles were measured to the maximum operational depth. In fall, the CTD/water sampler (Sea-Bird SBE 9) was equipped with a WetLabs ECO PUCK Triplet for chlorophyll fluorescence. In spring, CTD/water samples were collected using an Idronaut Ocean Seven 316 Plus (Idronaut S.R.L., IT) on a General Oceanics Inc. rosette. A correction factor of two was applied to the fluorometer data to obtain chlorophyll concentration (Roesler et al., 2017). Mixed layer depths (MLD, $\Delta\sigma\theta = 0.03\,kg\,m^{-3}$) were estimated following de Boyer Montégut et al. (2004). Geostrophic velocities and Brunt-Väisälä buoyancy frequencies (N^2) were calculated using the Gibbs-SeaWater Oceanographic Toolbox (GSW). The level of no motion was set to 500 m (IOC et al., 2010). Integrated chlorophyll was calculated from 1 to 150 m depths in 1 m bins. Noon-time euphotic zone depths (Z_{Eu}; 1% light level) were determined from downwelling spectral irradiance data obtained with a free-falling radiometer relative to in-air solar irradiation (HyperPro, Satlantic, KAN). In addition, we compare our CTD data with water mass characteristics in the Red Sea basin that were obtained during an extensive hydrographic survey from 17.1 to 27.9°N (September–October 2011) in the framework of a joint project of KAUST and Woods Hole Oceanographic Institution (WHOI) (Bower and Farrar, 2015).

2.3. Water sampling and analysis

Seawater samples were collected at 13–18 depths and targeted oceanographic features, including (1) the lowest oxygen concentrations (oxygen minimum zone, OMZ), (2) the transition zone from upper to deeper layers (defined here as 200 m), from (3) the bottom and (4) the top of the deep chlorophyll maximum layer, (5) the DCM, and (6) the surface mixed layer (SML).

Water samples for measurements of ammonium concentration [NH_4^+] were tapped directly from Niskin bottles into Falcon tubes and held at +4 °C. [NH_4^+] was measured underway using the orthophthaldialdehyde (OPA) method (Holmes et al., 1999; Taylor et al., 2007) after an incubation period of 2–4 h in the dark (Trilogy® fluorometer, CDOM/NH_4 module, Turner Designs, USA). Other nutrient samples were collected by gravity filtration from Niskin bottles through 0.2 µm filters (Nuclepore®, Whatman, UK). Aliquots of the filtrate were frozen to −20 °C onboard and stored at −80 °C in the laboratory. Dissolved nitrate (NO_3^-) and nitrite (NO_2^-; collectively = NO_x), phosphorus (PO_4^{3-}), and silicate ($Si(OH)_4$) concentrations were measured via continuous flow analysis (AA3 HR, SEAL, USA) following the designated methods. Lower limits of quantitation (LOQ) were ~0.020–0.025 µM (NH_4^+), 0.1 µM (NO_3^-), 0.05 µM (NO_2^-), 0.1 µM (PO_4^{3-}), and 0.2 µM ($Si(OH)_4$).

Samples for $\delta^{18}O_{SW}$ measurements were collected directly from Niskin bottles into borosilicate vials (Exetainer®, Labco, UK) and stored at room temperature. In the laboratory, the $\delta^{18}O$ of CO_2 was determined following the equilibration method (Horita et al., 1989; Seth et al., 2006) and a slight modification (i.e. He flushing after each sample) using a GasBench II coupled online with a DELTA V isotope ratio mass spectrometer (Thermo Fisher Scientific Inc., FRG). The CO_2 reference gas (grade 4.5) was calibrated against Vienna Standard Mean Ocean Water (VSMOW) and Standard Light Antarctic Precipitation (SLAP); data are shown relative to VSMOW. Long-term reproducibility of replicate measurements of an internal lab standard is ≤0.10‰ (1 SD). The average SD of the measurements was 0.09‰ ($N = 116$). The $\delta^{18}O_{SW}$ data were validated using the Global Seawater Oxygen-18 Database–v1.21 (Schmidt et al., 1999).

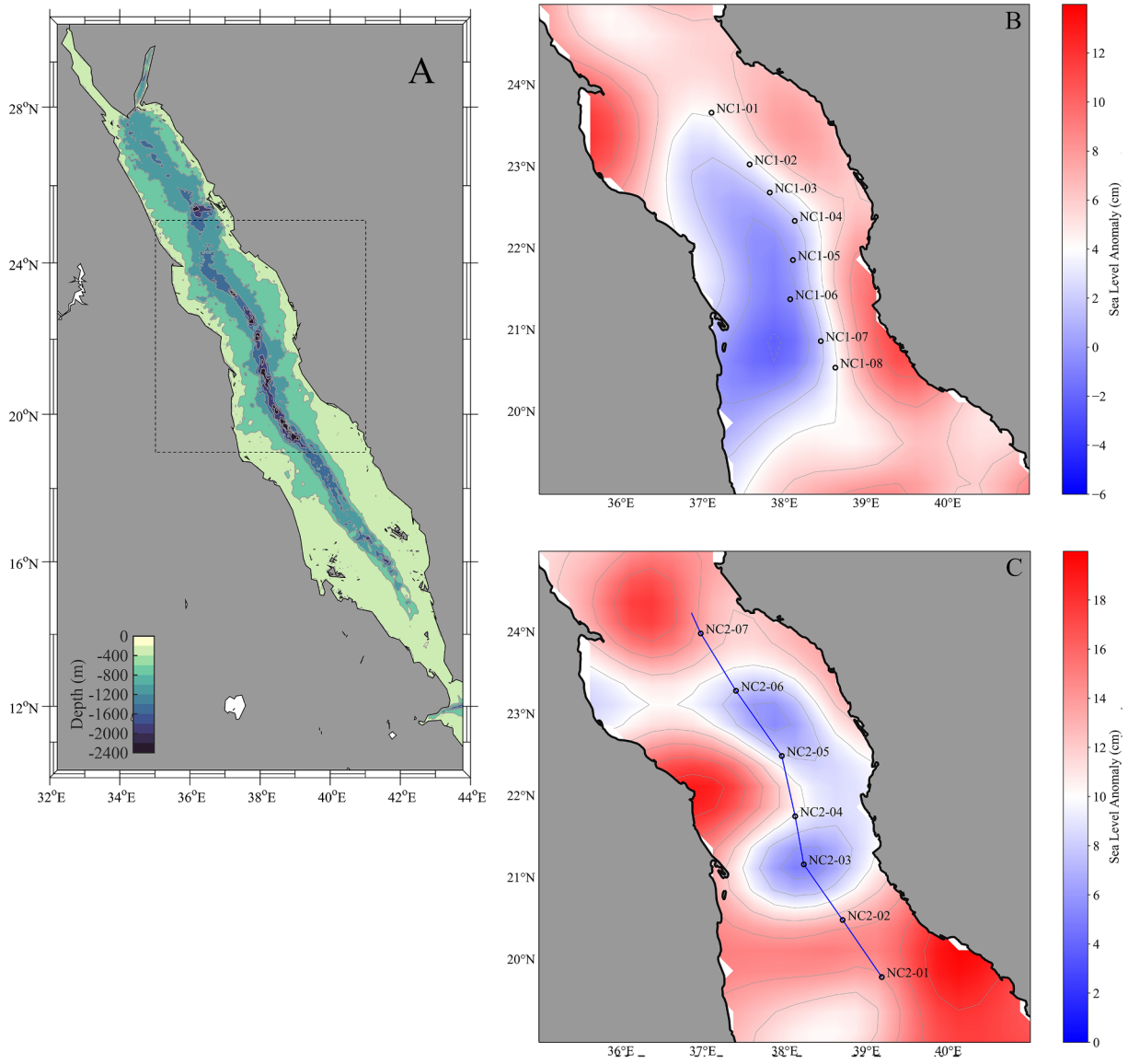

Fig. 1. Bathymetric map of the study region (A). Zoomed in maps of Sea Level Anomaly (SLA, cm) for each cruise period used for adaptive determination of positions for ship–based observations in the framework of the '*Nutrient Cycling in the Red Sea*' project in (B) fall 2014 (NC1), and (C) spring 2015 (NC2). The blue line in Fig. 1C indicates the preceding ScanFish survey track in spring 2015 carried out from 30 March–2 April 2015. The positions of occupied stations are listed in Table 1. (For interpretation of the references to colour in this figure legend, the reader is referred to the web version of this article.)

2.4. Plankton collections

Net-phytoplankton was collected between 9 and 11 am (local time = UTC + 3 h). A ring net (20 µm mesh size, non-filtering cod end; Hydro-Bios, FRG) was lifted vertically (0.5 m s^{-1}) from 160 m to the surface. Phytoplankton was preserved with Lugol's iodine solution and concentrated formalin (5% and 2% final concentration, respectively), and stored in amber glass bottles. Phytoplankton were counted using a Sedgewick-Rafter cell (LeGresley and McDermott, 2010). Only diatoms, dinoflagellates, microzooplankton (mostly heterotrophic loricate tintinnids), *Trichodesmium* (individual trichomes) and free-living *Richelia intracellularis* were identified and counted. Protozoa are referred to as a collective group of mixo-/heterotrophic dinoflagellates and microzooplankton (Stoecker and McDowell Capuzzo, 1990). Flow meter readings and mean values from triplicate enumerations (Cells m^{-3}) were used for quantitative data evaluation. We were aware that the phytoplankton community in the Red Sea cannot be fully examined using light microscopes alone because cells < 10 µm are difficult to quantify. Hence, additional water samples were collected from the DCM for complementary high-performance liquid chromatography (HPLC) analysis and pigment fingerprinting of the phytoplankton community (Supplementary Fig. 2, Supplementary Table 1). The degree of symbiotic endemism of *Richelia* with its host *H. indicus* was not assessed as this would have required further epifluorescence-microscopic studies (Villareal et al., 2012).

Zooplankton was collected after sunset with a ring net (55 µm mesh size, non-filtering cod end; Hydro-Bios) that was lifted vertically (0.5 m s^{-1}) from 160 m to the surface. Zooplankton was drained through 20 µm mesh and preserved (4% buffered formalin). Zooplankton samples were not collected at the two southernmost stations during NC1 due to adverse sea state. Counts were repeated three times on subsamples of 5 mL (> 200 individuals per subsample). Zooplankton data include Copepoda (adults, copepodites, nauplii), Chaetognatha, and veliger of Gastropoda and Bivalvia; 'other' zooplankton include Appendicularia, Decapoda larvae, Ostracoda, and Pteropoda. Adult Copepoda were determined to the genus/species level whenever possible (Kürten et al., unpub. data). Flow meter readings and mean values from triplicate enumerations (Ind. m^{-3}) were used for

Table 1
Station IDs for the two Nutrient Cycling (NC) cruises in fall 2014 and spring 2015, sampling positions and date, depth of the deep chlorophyll maximum (DCM), the 1% light level (Z_{Eu}) as determined by HyperPro measurements, salinity, potential temperature (°C, Theta), concentrations of dissolved oxygen, NO_x, PO_4^{3-}, $Si(OH)_4$, NH_4^+, and chlorophyll *a* at the DCM, the depth of the nitracline and the integrated chlorophyll *a* content calculated in 1 m bins in the upper 150 m. LOQ = concentration below limit of quantitation.

Cruise	Station ID	Latitude (°N)	Longitude (°E)	Sampling date	MLD (m)	DCM (m)	Z_{Eu} (m)	PSU	θ (°C)	O_2 (mg L^{-1})	NO_x (µM)	PO_4^{3-} (µM)	$Si(OH)_4$ (µM)	NH_4^+ (µM)	Chl *a* (mg m^{-3})	Nitracline depth (m)	Integrated chl *a* (mg m^{-2})
Fall 2014	NC1-1	23.6739	37.1034	20 October	4	94	80	40.164	24.097	4.0	LOQ	LOQ	0.90	0.064	0.31	110	15.9
	NC1-2	23.0398	37.5749	21 October	43	82	71	40.112	23.897	3.9	0.39	LOQ	1.10	0.029	0.33	99	11.8
	NC1-3	22.6958	37.8210	22 October	5	70	85	40.051	24.579	3.9	0.09	LOQ	0.90	0.014	0.35	78	16.5
	NC1-4	22.3486	38.1223	23 October	6	102	77	40.144	23.803	4.0	0.35	LOQ	1.10	0.044	0.25	112	11.7
	NC1-5	21.8689	38.0981	25 October	4	70	79	40.061	24.985	4.1	0.38	LOQ	1.00	0.039	0.16	97	11.2
	NC1-6	21.3889	38.0700	26 October	24	101	78	40.138	23.990	4.1	0.12	LOQ	1.00	0.038	0.26	117	10.6
	NC1-7	20.8758	38.4396	27 October	11	70	76	39.708	25.953	3.7	0.09	0.10	1.30	0.040	0.36	76	14.0
	NC1-8	20.5514	38.4396	28 October	5	70	80	39.681	25.831	3.7	0.06	LOQ	1.60	0.042	0.21	74	15.9
Spring 2015	NC2-1	19.8058	39.1870	3 April	5	70	72	39.194	26.022	5.8	1.67	0.20	1.40	0.064	0.39	93	12.4
	NC2-2	20.5022	38.7062	4 April	44	90	78	39.797	25.250	6.0	1.43	0.10	1.10	0.043	0.31	102	10.4
	NC2-3	21.1794	38.2429	5 April	30	78	73	40.236	24.094	4.3	1.06	0.08	1.00	0.048	0.33	117	9.1
	NC2-4	21.7708	38.1260	6 April	32	85	68	40.146	24.687	4.4	0.92	0.05	0.90	0.055	0.28	119	13.9
	NC2-5	22.5108	37.9642	7 April	26	58	72	39.854	25.037	4.3	0.60	0.05	0.90	0.070	0.39	123	21.1
	NC2-6	23.3031	37.4093	8 April	21	85	81	40.324	23.183	4.3	3.83	0.49	1.50	0.087	0.31	28	15.2
	NC2-7	23.9981	36.9707	9 April	6	100	87	40.306	22.921	4.4	0.5	0.0	1.0	0.105	0.29	93	13.6

quantitative data evaluation.

2.5. Nutrient data evaluation

Stoichiometric indices of nutrient supply and limitation have been derived from the oceanographic benchmark of Redfield et al. (1963) which depict the prevalence of biogeochemical conditions at large spatial scales. We calculated the semi-quantitative index $N^* = [NO_3^-] + [NO_2^-] - 16 \times [PO_4^{3-}]$ following Altabet (2006) and Deutsch and Weber (2012). A positive N^* points to an excess of N relative to P, whereas a negative N^* points to a deficit of N. These values reflect the net effect of N_2 fixation (which increases N^*) and denitrification (which decreases N^*). Complementarily, we refer to the index $Si^* = [Si(OH)_4] - ([NO_3^-] + [NO_2^-])$ that is informative about the production of algae that require Si for their growth such as diatoms and some Chrysophytes (Sarmiento et al., 2004). Section plots of nutrient concentrations and indices use linear interpolations (OriginPro 9). Due to the limits of quantitation, N^* and Si^* could not be computed for all sampling depths and stations. Outliers and extreme cases were considered as exceeding 3-times the interquartile ranges and removed. Mann-Whitney *U* tests were used to examine differences in nutrients and N^* and Si^* for the euphotic zone (1–200 m) between fall and spring. Comparison of physical and biogeochemical characteristics used one-way ANOVAs followed up by Tukey's post hoc tests to assess differences between stations (SPSS 25). The thickness of the nitracline was calculated by fitting a sigmoid function through in situ $[NO_3^-]$ from each station and used to determine the depth of the 10% and 90% bounds where the respective subsurface nutrient concentration was reached (Hauss et al., 2013). The nitracline depth was defined as the depth at which the $[NO_3^-]$ reached 1 µM (Painter et al., 2007; Bonnet et al., 2013). All regressions were significant, and the adjusted R^2 values ranged from 0.96 to 0.99 (OriginPro 9.0). The average $[NO_3^-]$ in the nitracline was calculated from in situ values falling into the depth range of the nitracline. Station information and environmental conditions are summarized in Table 1.

3. Results

3.1. Seasonality in water column structure

3.1.1. Stratified fall conditions

For fall 2014, the SLA image gives the appearance of a tilted sea surface from 20 to 23°N with a depression on the western half of the Red Sea basin and an elevation along the eastern side toward the Arabian Peninsula (Fig. 1B). This structure is consistent with a northward flowing current that underlies the general northbound thermohaline summer circulation. The vertical distribution of water masses in the upper 100 m shows that cooler, saltier water is observed in the north, and relatively warmer, less saline water in the south (Fig. 2A and B). The DCM was primarily at ~80 m depth, but observed deeper at station NC1-4 and NC1-6 (Table 1). There was no significant difference in integrated chlorophyll concentrations in the euphotic zone between stations ($F_{(7,68)} = 0.632$, $p = 0.727$) despite a localized increase in the south. At NC1-3 there was a patch of water with a secondary subsurface chlorophyll maximum at around 120 m (Fig. 2D). At the southern two stations there is an indication of low salinity ($F_{(7,68)} = 1.231$, $p = 0.042$, as revealed by Tukey's post hoc comparisons of stations), and relatively warmer water between 50 and 75 m depth. It coincided with high chlorophyll concentrations at NC1-7 and NC1-8 (~0.38 µg L^{-1}). Lowest chlorophyll concentrations (~0.05 µg L^{-1}) were measured in the SML at NC1-4 and NC1-6 (Fig. 2D). Oxygen concentrations were similar across stations ($F_{(7,68)} = 1.290$, $p = 0.269$), reaching maximum values in the mixed layer at NC1-3 (4.72 mL L^{-1}; Fig. 2C). Oxygen concentrations decreased with depth, reaching low concentrations down to 0.39 mL L^{-1} at the OMZ (Fig. 2C). A region of subsurface oxygen maximum exists in the upper layer at the DCM. The geostrophic

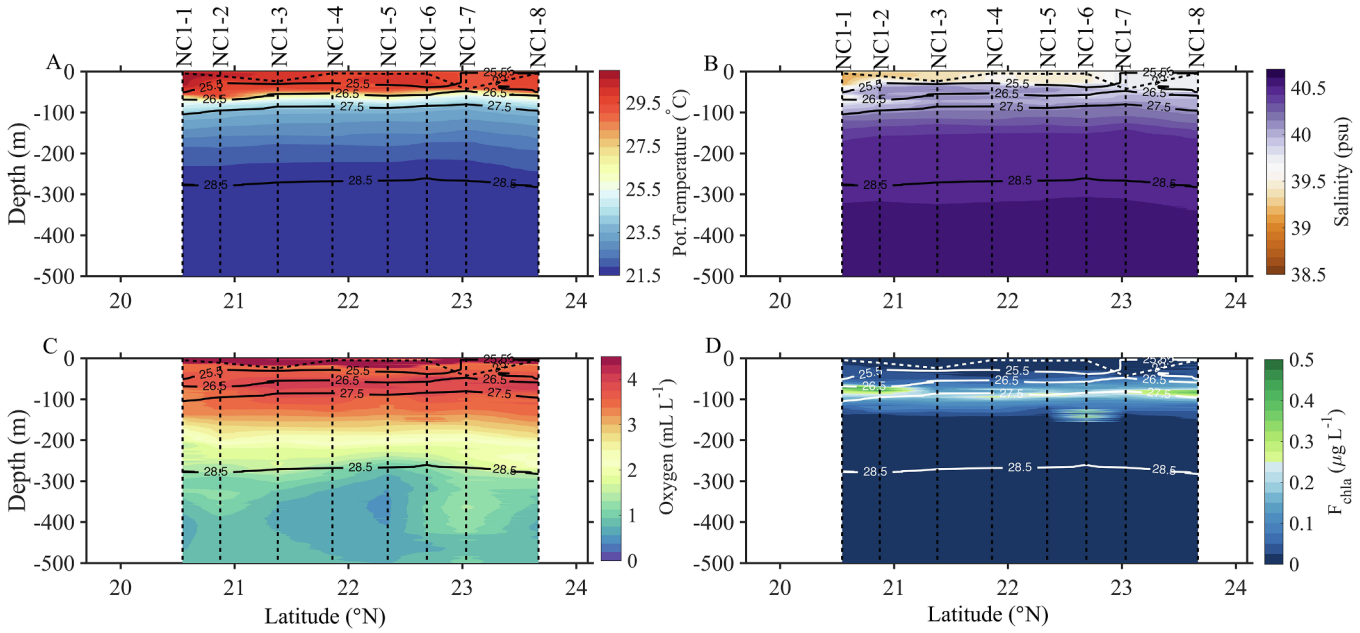

Fig. 2. Regional North–South CTD transect along the cruise track in fall 2014 (NC1 cruise) as shown in Fig. 1B. (A) Potential temperature (°C), (B) salinity, (C) oxygen (mL L^{-1}), (D) chlorophyll fluorescence (μg L^{-1}). For all panels, isopycnals are shown as contour lines at 0.5 kg m^{-3} intervals. Locations of the sampling stations are marked with vertical dashed black lines. Horizontal dashed lines indicate the mixed layer depths. (For interpretation of the references to colour in this figure legend, the reader is referred to the web version of this article.)

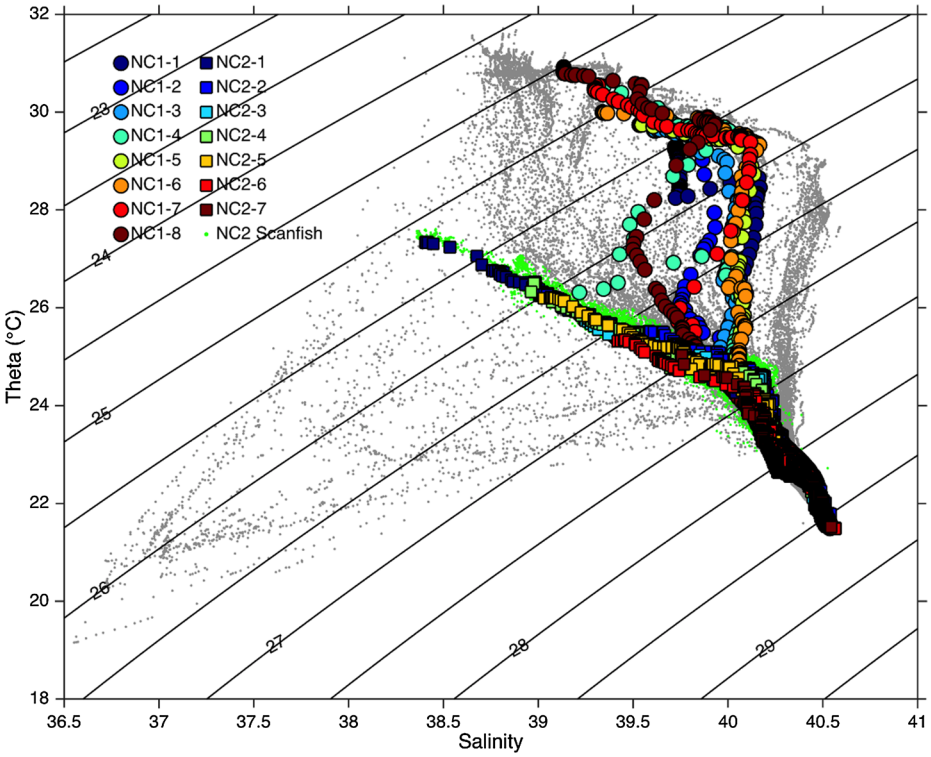

Fig. 3. *T–S* diagram. Temperature–salinity plot with density contours from the fall (circles) and spring (squares) surveys in the central Red Sea indicated with the progression from deep blue (north) to deep red (south). The ScanFish data are shown in green. The subjacent *T*−*S* data (grey dots) are taken from a KAUST–WHOI hydrographic survey carried out in September–October 2011 from 17.1 to 27.9°N (Bower and Farrar, 2015). (For interpretation of the references to colour in this figure legend, the reader is referred to the web version of this article.)

velocity in this region suggests a northeastward flow between 22.9 and 23.3°N (data not shown). The eastward transport of water may be indicative of an anticyclonic feature to the east of NC1-2. The pycnocline also deepens at the southern two stations, but this variation in pycnocline depth is not fully resolved. It remains uncertain whether this is part of a larger eddy-like feature or whether it may simply be a meridional gradient within the Red Sea. Variations in temperature and salinity below 300 m were not discernable (Fig. 2A and B) and the study area is well stratified below 200 m as indicated by Brunt–Väisälä frequencies (data not shown). In addition, the *T–S* data from the KAUST-WHOI hydrographic survey helps identifying the water masses that are present in this study. The comparison with our CTD observations shows the presence of GASW in fall 2014 (Fig. 3).

3.1.2. Eddy activity in spring

In spring, two mesoscale cyclonic eddies were detected, of which the first centered at 21.2°N and the second at 23°N (Fig. 1C). The SLA data also indicate the presence of two anticyclonic features at the

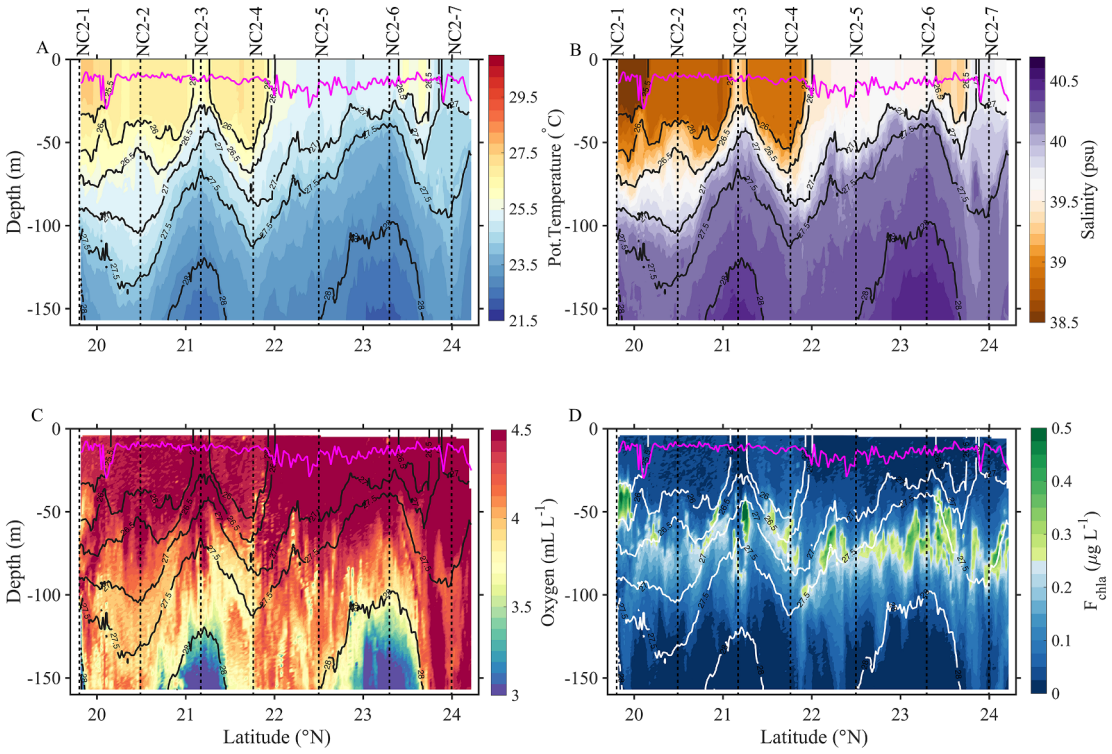

Fig. 4. Distribution of physical and chemical properties along the ScanFish track in spring 2015 (NC2 cruise) as shown in Fig. 1C. (A) Potential temperature (°C), (B) salinity, (C) oxygen (mL L^{-1}), (D) chlorophyll fluorescence (μg L^{-1}). For all panels, isopycnals are shown as contour lines at 0.5 kg m^{-3} intervals. Locations of the sampling stations are marked with vertical dashed black lines. The magenta line represents the mixed layer depth. (For interpretation of the references to colour in this figure legend, the reader is referred to the web version of this article.)

southern and northern ends of the survey area, at 20°N and 24.5°N, respectively. Latitudinal gradients in temperature and salinity were observed from the south to the north (Fig. 4A and B). At the southern end of the ScanFish survey, warm (< 27 °C) and low salinity water (38.5 psu) was found in the upper 25 m. The *T–S* characteristics indicate the presence of GASW and its modification under the influence of mixing and evaporation in upper layers (Fig. 3). The gradient of thermohaline characteristics identified the transport of GASW to the North, its interaction with mesoscale features (i.e. the cyclonic eddies), and entrainment of the low salinity water into the surface circulation (Fig. 4). No significant changes in thermohaline and dynamic characteristics of the region were observed between the time of the ScanFish survey and subsequent CTD/water sampling (Supplementary Fig. 3).

Seawater oxygen stable isotopes ($\delta^{18}O_{SW}$) traced the lateral advection of GASW in the upper layers of the Red Sea (Fig. 5). In the central Red Sea, $\delta^{18}O_{SW}$ ranged from 1.4 to 2.3‰. The GASW is associated with relatively low $\delta^{18}O_{SW}$ and affected by evaporation and mesoscale features. At NC2-1, low $\delta^{18}O_{SW}$ (1.5‰ at 50 m) coincide with increased chlorophyll concentrations between 35 and 55 m (Fig. 4D). The lowest $\delta^{18}O_{SW}$ was found at 10 m depth at NC2-4 and indicates the presence of GASW well below Z_{Eu}, concurrent with a depression of the 27 kg m^{-3} isopycnal at the periphery of the cyclonic eddy and a second DCM at ~67 m (Supplementary Fig. 3). Consistent with the eastward transport of water by the cyclonic features centered at 21.2°N and 23.3°N, velocities show alternating directions of geostrophic currents along the survey track (data not shown). On average, the velocity was uniform through the upper 50 m of the water column and then decreased from 50 to 200 m to less than 30% of the surface velocity.

Over the cruise period, strong winds (> 15–25 knots) prevailed until 7 of April 2015 causing weakening of the stratification (based on Brunt-Väisälä frequencies, N^2, data not shown). Vertical distributions of temperature, salinity, density, oxygen, and $\delta^{18}O_{SW}$ indicate shallowing of cooler, saltier, denser, and lower oxygen water in the center of two

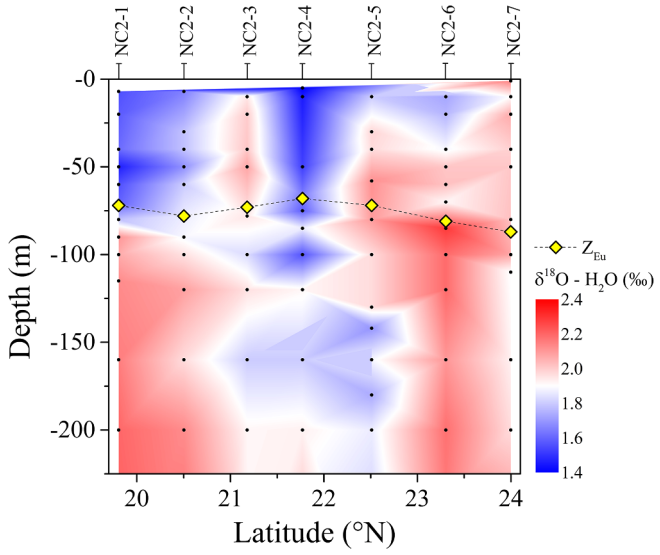

Fig. 5. Vertical sections of seawater oxygen stable isotopes ($\delta^{18}O_{SW}$, ‰) in spring 2015. Rhombic symbols indicate the depths of the 1% light level (Z_{Eu}). Black dots indicate sampling depths. (For interpretation of the references to colour in this figure legend, the reader is referred to the web version of this article.)

cyclonic eddies (Figs. 4 and 5). The deepening of the DCM at the boundaries of these cyclonic structures (i.e. NC2-2: DCM ~90 m) cause a break in the chlorophyll and oxygen distribution, with the DCM between 40 and 80 m (Fig. 4D). The lowest chlorophyll concentration was observed in the SML at the edge of the anticyclonic eddy at ~24.5°N (NC2-7: ~0.2 μg L^{-1}), whereas the maximum chlorophyll concentration (~0.5 μg L^{-1}) occurred at 60–75 m in the cyclonic eddy between

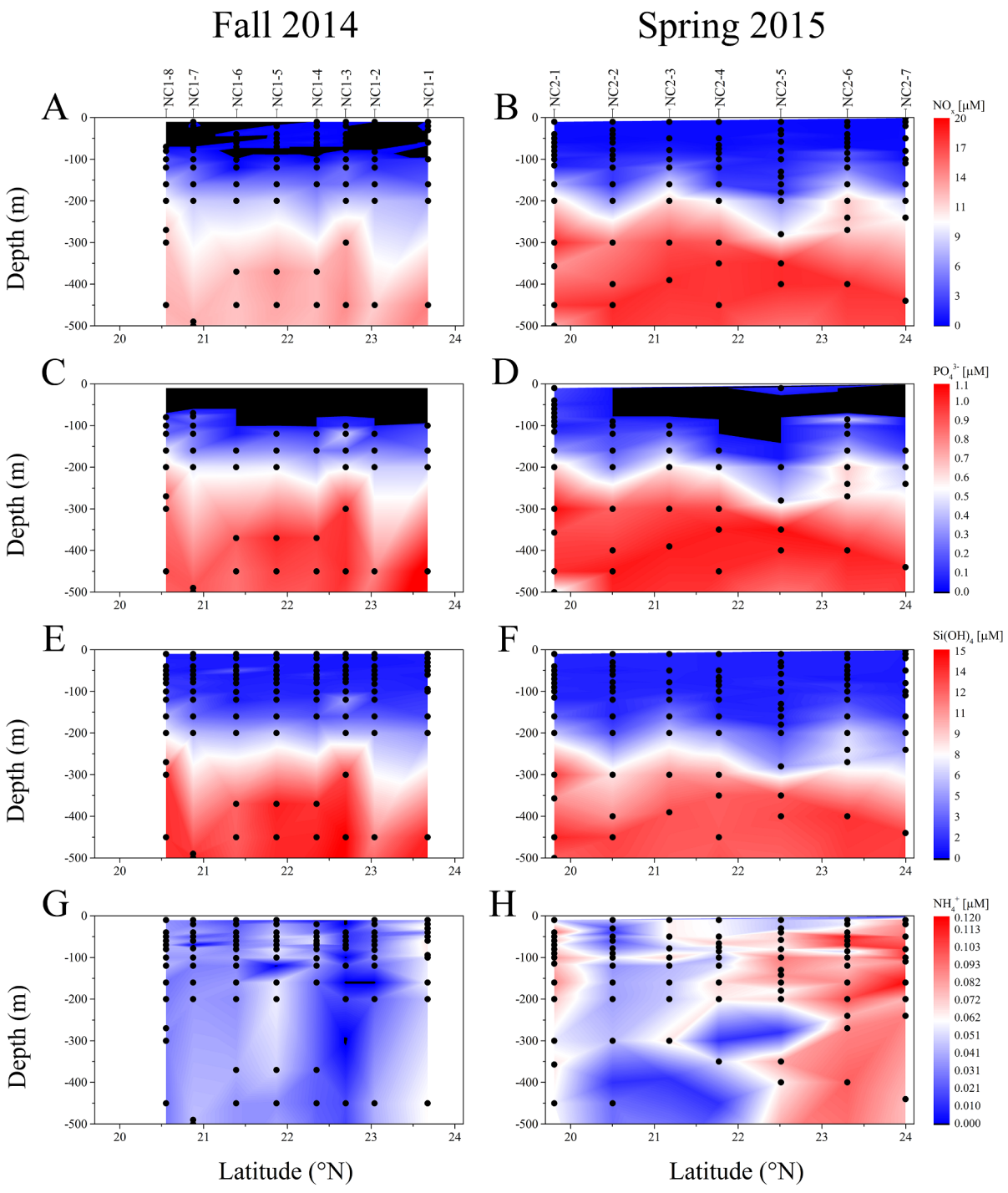

Fig. 6. Vertical sections of dissolved inorganic nutrient concentrations in the upper 500 m of the water column in fall 2014 (left panels, NC1 cruise) and spring 2015 (right panels, NC2 cruise). (A, B) NO_x, (C, D) PO_4^{3-}, (E, F) $Si(OH)_4$, and (G, H) NH_4^+. Station IDs are indicated above the upper panels. Black dots indicate discrete sampling depths. (For interpretation of the references to colour in this figure legend, the reader is referred to the web version of this article.)

22.5°N and 23°N (Supplementary Fig. 3).

Despite significant differences between the two seasons in salinity, temperature, and oxygen concentration, the chlorophyll concentrations were similar (Supplementary Table 2). Overall, the depths of the DCM in the central Red Sea was similar during the two cruises and only slightly shallower in spring (~81 ± 14 m, range = 58–100 m) than in fall (~82 ± 15 m, range = 70–102 m). Concurrent with regular seasonal changes in SST (Supplementary Fig. 1), ship-based observations of temperatures in the upper layer were higher in fall, whereas oxygen concentrations were higher in spring (Supplementary Table 2).

3.2. Spatial distribution of nutrients

The distribution and relative proportions of nutrients in the Red Sea was related to the hydrographic conditions and dynamic processes. From the surface to the OMZ layer [NO_x], [PO_4^{3-}] and [$Si(OH)_4$] increased (Fig. 6A–F). In fall, [NO_x] and [PO_4^{3-}] were depleted above the nitracline below the limits of quantification at many stations (Fig. 6A and C). Considering the central Red Sea as a whole, [NO_x], [$Si(OH)_4$] and [NH_4^+] differed between fall and spring (Supplementary Table 2). The mean [NH_4^+] in fall was lower than in spring, whereas [PO_4^{3-}]

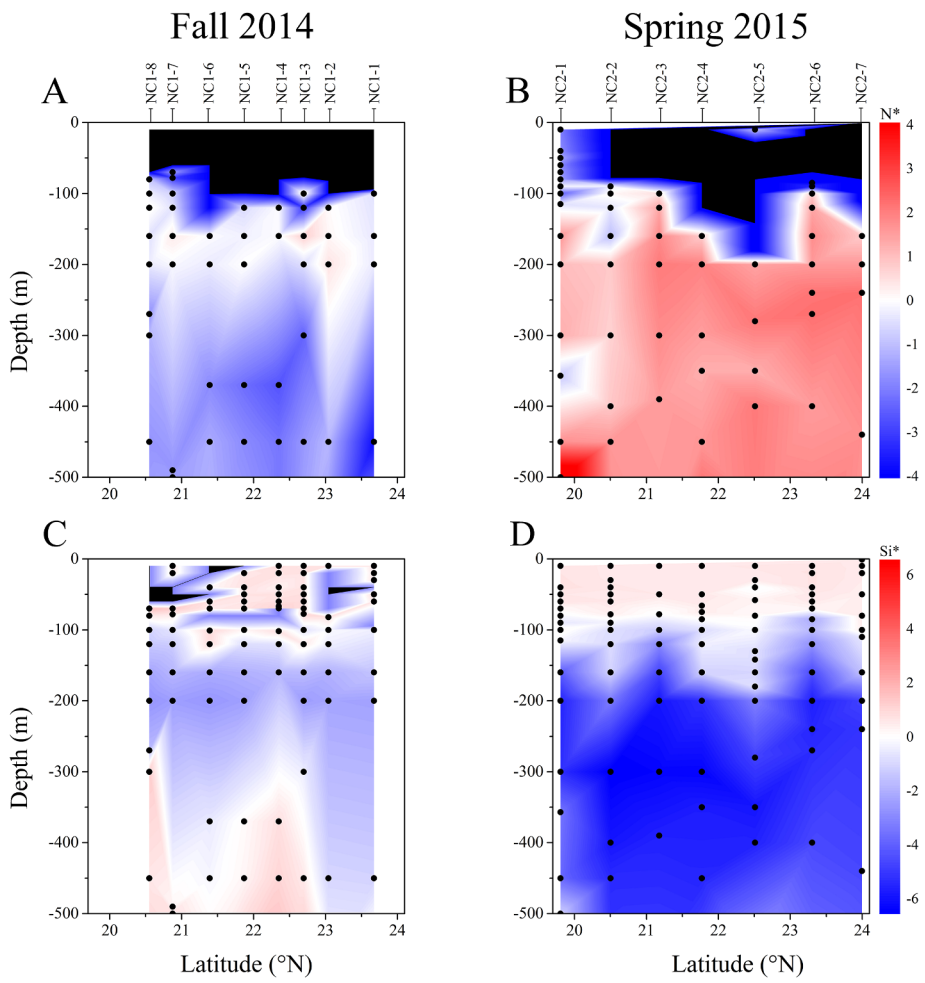

Fig. 7. Profiles of likely nutrient limitation indices of dissolved nitrogen (N^*) (A, B) and silicic acid (Si^*) (C, D) in the upper 500 m of the water column along the latitudinal gradient in fall 2014 (right panels) and spring 2015 (left panels). Black dots indicate discrete sampling depths. (For interpretation of the references to colour in this figure legend, the reader is referred to the web version of this article.)

were similar. In fall, [NH_4^+] were highest at station NC1-1 (0.055 ± 0.011 µM) and lowest at NC1-3 (0.014 ± 0.003), and both differed significantly from the other stations (NC1: $F_{(7,91)} = 22.937$, $P < 0.001$; individual Tukey's tests not shown). In spring, [NH_4^+] were significantly higher at stations NC2-5 to NC2-7 and lowest at NC2-2 (NC2: $F_{(6,87)} = 16.410$, $P < 0.001$; Fig. 6G and H). Higher [NH_4^+] were present in the upper 200 m at NC2-1. The spatial pattern of nutrient upwelling in spring was not coherent with the NH_4^+ data.

Euphotic zone N^* and Si^* were lower in fall than in spring, even though N^* could not be calculated for all depths due to the limits of quantification. N^* did not exceed 0.7 µM in fall but reached up to 2 µM in spring at 200 m depth at NC2-3 (Fig. 7A and B). Si^* indicated some Si $(OH)_4$ deficiency in the euphotic zone during both seasons; however Si $(OH)_4$ was strongly depleted in the aphotic zone in spring (Fig. 7C and D). We note clear differences between the euphotic and the aphotic zone for both N^* and Si^*, albeit no difference in Si^* in fall.

The 28 kg m^{-3} isopycnal was associated with the upper bound of the nitracline and set a shallow limit to the nutrient availability. The nitracline extended over a wider depths range in fall (~149.5 ± 26.0 m) than in spring (~125.9 ± 33.5 m; Fig. 8A and B). Within a few meters above the upper bound of the nitracline a concentration of ~1 µM [NO_3^-] was reached. On average Z_{Eu} was ~78.1 ± 4.3 m in fall and ~75.9 ± 6.5 m in spring. With one exception at NC2-6, Z_{Eu} was above the nitracline and did not correlate well with the DCM (Pearson $R_{Fall} = 0.739$, $P = 0.058$; $R_{Spring} = -0.335$, $P = 0.463$; Fig. 8A and B).

3.3. Modulation of phytoplankton communities

3.3.1. Fall

The phytoplankton community responded to seasonal changes in water mass characteristics, mesoscale activity, and nutrient availability. High abundances of dinoflagellates in fall were reflected in a mean (± SD) diatom:dinoflagellate ratio of 0.5 ± 0.1 across stations and depletion of N and P in the euphotic zone (Fig. 8A). The most abundant dinoflagellate species was the heterotrophic *Podolampas palmipes* (1940 ± 1185 Cells m^{-3}) which was present at NC1-3–NC1-8 (species-specific data not shown). Conversely, *P. palmipes* was absent where GAIW was observed. The most abundant diatom species was *Hemiaulus indicus* (972 ± 742 Cells m^{-3}). We identified *Rhizosolenia-Richelia* DDAs at NC1-1–2 and NC1-4–5. We also document higher counts of microzooplankton (7-fold) and *Trichodesmium* (10-fold) in fall than in spring (Fig. 8C and D). *Trichodesmium* was present on average with 19,923 ± 8138 trichomes m^{-3} and reached highest counts at NC1-4 (31,293 trichomes m^{-3}).

The 25.5 kg m^{-3} isopycnal rose near to the surface at 23°N (Fig. 8A) which is consistent with a westward geostrophic velocity at NC1-2 and eastward velocity at NC1-1. Here, dinoflagellates and microzooplankton were most numerous (47,005 and 35,253 Cells m^{-3}, respectively; Fig. 8C). This observation could be due to advection from populations from the west, an uplift from subsurface layers, or due to changes in the plankton communities in the shear zone between the boundary current and the anticyclonic eddy to the north of the survey area.

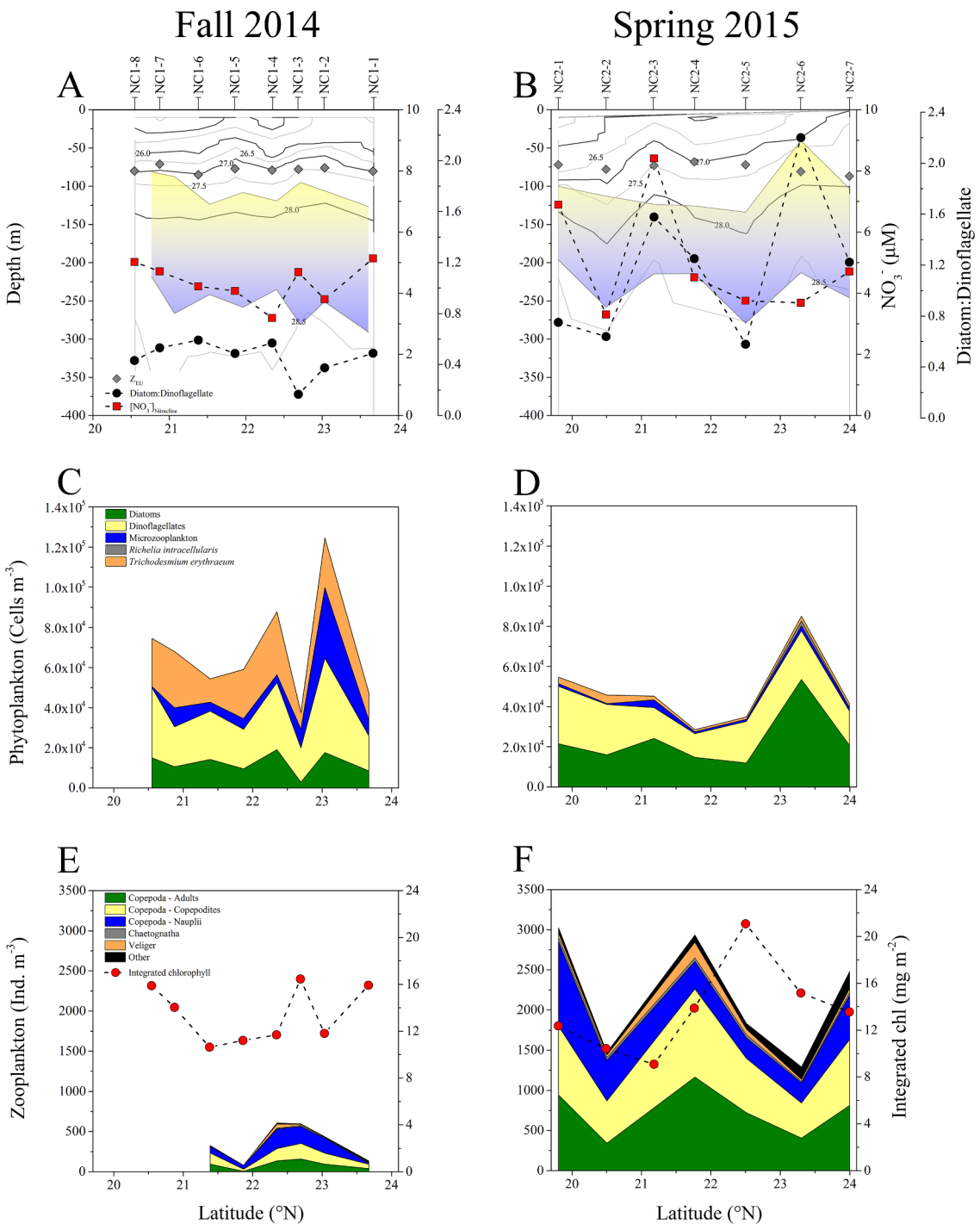

Fig. 8. Environmental conditions and modulation of phytoplankton and zooplankton abundances during the cruises in fall 2014 (left panels, NC1 cruise) and spring 2015 (right panels, NC2 cruise). (A, B) Extent of the nitracline (shaded area), 1% light level (Z_{Eu}) determined by HyperPro measurements, diatom:dinoflagellate ratio, and mean NO_3^- concentrations within the nitracline. Density contours lines at 0.5 kg m^{-3} intervals are shown for visualization of stratification and upwelling. (C, D) Distribution of microphytoplankton (Cells m^{-3}), and (E, F) distribution of zooplankton (Ind. m^{-3}), and integrated chlorophyll (mg m^{-2}). Station IDs are indicated above the upper panels. (For interpretation of the references to colour in this figure legend, the reader is referred to the web version of this article.)

The stratification in fall limits the nutrient variability, and only small variations of $[NO_3^-]$ (≈4.4 ± 0.7 µM) within the nitracline occurred. Increasing $[NO_3^-]$ in the nitracline were positively correlated with integrated chlorophyll (Pearson $R = 0.792$, $P < 0.019$, $N = 8$). A higher integrated chlorophyll concentration at NC1-3 (16.5 mg m^{-2}) coincided with a slight elevation of the 28.5 kg m^{-3} isopycnal to ~ 260 m, increased zooplankton, and reduced phytoplankton abundances (Fig. 8A, C and E).

3.3.2. Spring

In spring, the mean (± SD) diatom:dinoflagellate ratio increased to 1.2 ± 0.6, and was higher in the center of the cyclonic eddies at 21.3°N and 23.3°N (Fig. 8B and D). The most numerous diatom and dinoflagellate taxa were *Hemiaulus membranaceus* (mean ± SD: 1,861 ± 1,401 Cells m^{-3}) and the heterotrophic *Protoperidinium elegans* (1,012 ± 907 Cells m^{-3}), respectively. *Trichodesmium* was present at all stations (2228 ± 1159 trichomes m^{-3}), whereas

Rhizosolenia-Richelia associations were not observed. *Trichodesmium* were more numerous at NC2-2 (4176 trichomes m^{-3}) and NC2-6 (2432 trichomes m^{-3}) (Fig. 8D). In addition, microzooplankton abundances averaged 1650 ± 541 Cells m^{-3}.

The mesoscale eddy activity uplifted the isopycnals at NC2-3 and NC2-6. The uplift led to higher nutrient availability in the euphotic zone at NC2-3 and increased counts of the diatoms *Thalassiosira subtilis* (2362 Cells m^{-3}) and *Pseudo-nitzschia cuspidata* (1772 Cells m^{-3}). The peaking abundance of *Thalassiosira* could be responsible for the increased biomass of diatoms at NC2-3 (~20% of total chlorophyll; Supplementary Fig. 2, Supplementary Table 1). The 28 kg m^{-3} isopycnal also indicated an uplift of nutrients at NC2-6 which is consistent with a high abundance of diatoms (53,514 Cells m^{-3}). However, nutrients may have already been drawn-down which may help explain the increased numbers of the putative DDA *Hemiaulus* (7297 Cells m^{-3}) and presence of free-living *R. intracellularis* (2432 Cells m^{-3}). In addition, the cyclonic eddy at NC2-6 interacted with a patch of GASW as indicated by $\delta^{18}O_{SW}$ (~1.8‰; Fig. 6). At NC2-5, the 90% nitracline bound and the OMZ were deep (279 m and 550 m, respectively), and the phytoplankton abundance was reduced (Fig. 8B and D). We also observed the highest integrated chlorophyll concentration (21.1 mg m^{-2}) at this station due to multiple subsurface chlorophyll maxima at 58, 90, and 130 m. The relaxation of the wind after 7 of April 2015 allowed *Trichodesmium* to aggregate at the surface despite low integrated chlorophyll (Fig. 9F, Supplementary Fig. 4).

3.4. Modulation of zooplankton communities

Like phytoplankton, the zooplankton community was similarly influenced by seasons. Zooplankton abundances changed markedly from fall (364 ± 225 Ind. m^{-3}) to spring (2175 ± 746 Ind. m^{-3}; Fig. 8E and F; Supplementary Table 3). However, zooplankton abundances were loosely linked to integrated chlorophyll concentrations (NC1: Pearson $R = 0.227$, $P < 0.665$, $N = 6$; NC2: Pearson $R = 0.085$, $P < 0.872$, $N = 6$). Copepoda were the most numerous zooplankton group, to which Nauplii and copepodites stages contributed considerably. Among the most numerous adult copepods were *Parvocalanus crassirostris* (Calanoida), *Oncaea media* (Poecilostomatoida), and *Oithona plumifera* (Cyclopoida). In spring, Appendicularia and larval Decapoda contributed considerably to the category zooplankton 'other'.

Along the entire transect, the 28 kg m^{-3} isopycnal (at ~130 m) set the upper bound for the availability of deep nutrients. Aforementioned is consistent with limited phytoplankton growth and low zooplankton counts (Fig. 8D and F). Increased zooplankton counts at NC2-1 and NC2-4 were associated with GASW. In spring the highest numbers of *P. crassirostris* were found at NC2-4, whereas in fall *P. crassirostris* were most numerous at NC1-6. Higher quantities of zooplankton were also counted at the edge of the anticyclonic eddy (NC2-7; Figs. 1C and 8F). Notable were low zooplankton counts in the presence of an elevated integrated chlorophyll concentration at NC2-5 (21.1 mg m^{-2}; Fig. 8F).

4. Discussion

The goal of the present study is to ascertain how variability in upper layer dynamics regulates the biogeochemistry in the Red Sea and the associated changes in phytoplankton and zooplankton communities at the genus/species level. By linking abundances and biodiversity of phytoplankton and zooplankton communities as well as their competition for resources with physical dynamics (i.e. inflow of water from the Gulf of Aden, stratification, and mesoscale activity) we can understand the drivers of ecosystem metabolism in the Red Sea (Fig. 9). In brief, the strength of stratification varies between fall and spring and directly affects the nutrient availability between the upper layers with the interior. However, lateral advection of GAW and mesoscale eddy activity, as well as biological activity, i.e. microbial remineralization and diazotrophic N_2 fixation (*Trichodesmium* and DDAs), modulate the nutrient availability. The ecological relevance of dust input for nutrient cycling is also considered.

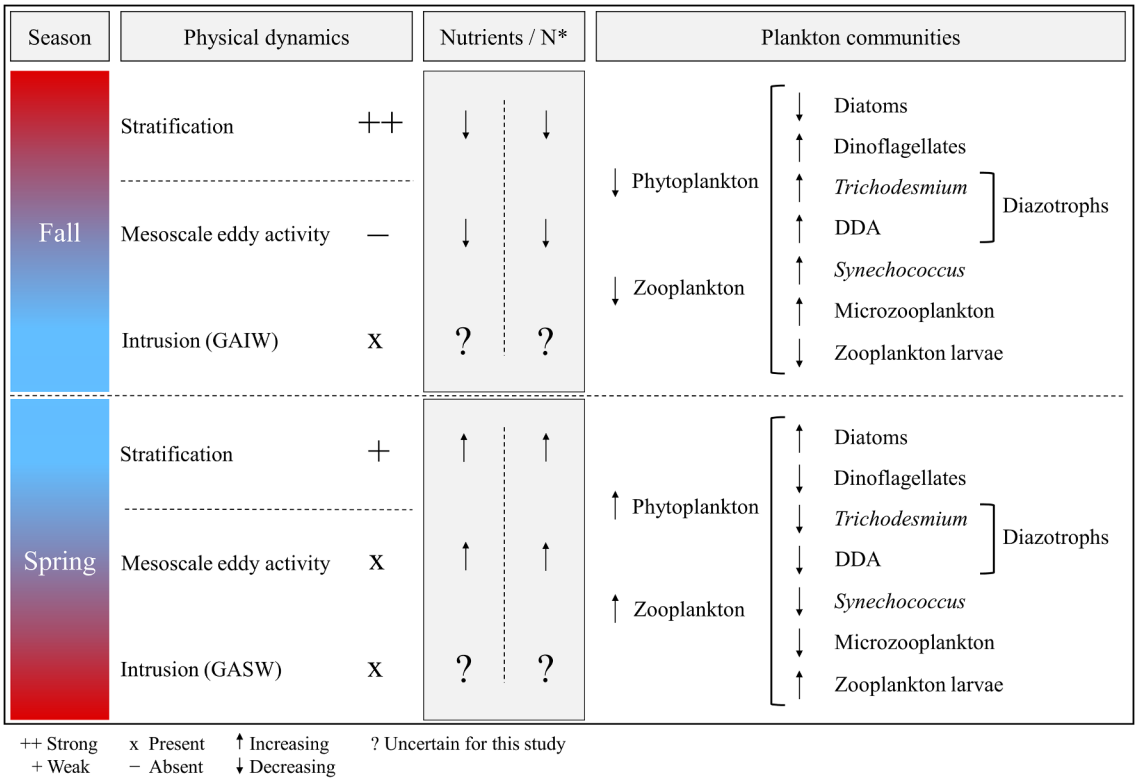

Fig. 9. Overview about the interplay between physical dynamics, nutrient availability and stoichiometry (N^*), and the composition of the plankton community as observed in fall 2014 and spring 2015 in the central Red Sea.

4.1. Upper layer processes in the Red Sea

The changes in the wind field associated with the monsoon reversal (Abualnaja et al., 2015) alter the exchange flow with the Gulf of Aden across the Bab-al-Mandab Strait from two layers in winter to three layers in summer and influence the primary production in the Red Sea (Halim, 1969; Patzert, 1974; Sofianos et al., 2002; Raitsos et al., 2015). The comparison of our in situ observations between fall 2014 and spring 2015 reveal how physical dynamics alter the phytoplankton and zooplankton identity. The fall cruise was carried at the end of the summer monsoon when the central Red Sea was strongly stratified. During this period, the supply of nutrients from below the nitracline was limited. In contrary, weak stratification and high horizontal geostrophic shear in spring were associated with mesoscale eddy structures. The latter enhanced the nutrient availability in the upper layer.

In this study, the presence of GAW was observed in both seasons. The *T–S* diagram (Fig. 3) supports the presence of GAIW at the southernmost station in fall. Although the inflow in summer transports nutrients into the Red Sea (Souvermezoglou et al., 1989), the nutrient concentrations in GAIW at NC1-8 were not increased, most likely due to uptake during its transport to the north. Though, in our study the observed higher chlorophyll concentration at NC1-7 and NC1-8 (Fig. 2D) is due to the lateral advection of GAIW in the central Red Sea. The SLA data (Fig. 1B) add further evidence of an upper-layer northward flow along the eastern boundary of the Red Sea (Bower and Farrar, 2015; Zarokanellos et al., 2017a). In contrast, thermohaline characteristics reveal the presence of GASW and its interaction with cyclonic mesoscale eddies in spring. Our observations of the present study concurred with recent descriptions of cyclonic eddy structures (Kürten et al., 2016; Zarokanellos et al., 2017a, 2017b). Since lower $\delta^{18}O_{SW}$ are typical for the Gulf of Aden and the adjacent Indian Ocean (Craig, 1966; Ganssen and Kroon, 1991), the $\delta^{18}O_{SW}$ of GASW patches reveals that (1) GASW can be traced in the Red Sea by its $\delta^{18}O_{SW}$, and (2) advect at least as far as 23.5°N (Figs. 3 and 6). Moreover, the role of eddies in the distribution of GASW is evident in the detection of low $\delta^{18}O_{SW}$ to over 100 m depths at station NC2-4 and attributable to the deepening of GASW at the periphery of the cyclonic eddy (Figs. 1B and 4). Hence, as suggested by Zarokanellos et al. (2017b), the present study also demonstrates that GASW entrains water from the northward flowing GAW around the periphery of eddies in the central Red Sea.

Some differences in the vertical distribution of chlorophyll were observed between the ScanFish tow and the hydrographic stations. At the southern end of the ScanFish survey, the DCM was much shallower (~42 m) and attained higher chlorophyll concentrations (> 0.65 µg L^{-1}) than in the northern region where the DCM was deeper (~75 m), and the maximum chlorophyll concentrations were ~0.5 µg L^{-1}. This difference may be attributable to relatively high spatial variability associated with the subsurface chlorophyll distribution that the ScanFish survey revealed (Fig. 4D). Besides, observations with high spatial and temporal resolution are needed to improve our understanding of mesoscale processes in the Red Sea. We advocate that low sampling frequency from widely-spaced CTD/water stations conceals the complex hydrodynamics in the ecosystem, see McGillicuddy et al. (1998) and Wilby et al. (2017). Such inaccuracy can be exemplified by comparing, for example, the ScanFish sections (Fig. 4) with the CTD profiles (Supplementary Fig. 3): the high-resolution ScanFish measurements reveal the patchiness of GASW that was not apparent in the CTD data. Even more critical, the ScanFish survey captured a 20 km wide 'chimney' of salty and colder water in the center of the cyclonic eddy located at 21.3°N. This feature may not have been sampled for our study had we not already known of its presence from the ScanFish survey. Furthermore, the high resolution data shows significant heterogeneity in the oxygen and chlorophyll distributions, much more than is apparent in the temperature and salinity data, and which is not captured from the more broadly-spaced hydrographic profiling. Thus, high resolution measurements from ship-based ScanFish surveys and autonomous gliders are better suited to resolving the importance of mesoscale and submesoscale structures in the Red Sea compared to (non-adaptive and traditional) ship-based station profiles and sections.

4.2. Biological responses of plankton communities

The annual plankton cycle in the Red Sea is chiefly affected by the Indian Ocean's monsoon as it influences the circulation and the associated lateral intrusion of GAW, strengths of stratification/mixing, and mesoscale eddy activity (Shaikh et al., 1986; Bower and Farrar, 2015). Two main periods can be differentiated in the seasonal cycle. Raitsos et al. (2013) showed that the most productive period starts in mid-October (fall, see Section 4.2.1) and ceases between March and April (spring, see Section 4.2.2). The phytoplankton and zooplankton communities differed markedly between fall 2014 and spring 2015 in response to physical processes and nutrient availability. Low nutrient availability and zooplankton abundance, and concomitant higher microzooplankton and dinoflagellates counts in fall point toward increased microbial activity and the microbial loop *sensu* (Azam et al., 1983). In contrast, higher abundances of diatoms and reduced number of microzooplankton suggest a predominantly autotrophic food web architecture.

4.2.1. Plankton community in fall

The plankton community in the central Red Sea in fall mostly resembled the type III domain of phytoplankton *sensu* Wyatt (2014) which typically features a range of nutrient acquisition strategies and a wide variety of life strategies. A type III phytoplankton community is characteristic of offshore waters where summer heating and weak winds lead to stratification and depletion in nutrients, and ultraphytoplankton (< 5 µm) mixo-/heterotrophic phytoplankton and N_2 fixation become dominant (Wyatt, 2014). During the nutrient deficient period in fall, ultraphytoplankton has an ecological advantage due to higher uptake efficiency of remaining and recycled nutrients. Since *Synechococcus* live primarily on NH_4^+ and urea and not NO_3^- (Moore et al., 2002), uptake and regeneration of NH_4^+ by the microbial loop may help explaining the larger biomass of *Synechococcus* in fall (Supplementary Fig. 2, Supplementary Table 1). Significantly higher abundances of high nucleic acid bacteria in the upper 200 m (fall: 113,193 ± 62,072 Cells mL^{-3}, spring: 59,249 ± 31,141 Cells mL^{-3}; $U = 2959$, $p < 0.001$; A. Moran, pers. comm.) also support the greater importance of microbial recycling for primary producers (regeneration production) in fall.

The nutrient depleted conditions in fall increased the numbers of diazotrophic phytoplankton, i.e. *Trichodesmium* and DDAs. Large numbers of *Trichodesmium* occurred where SST and surface sea temperatures (10 m) indicates temperatures > 30.5 °C (Supplementary Fig. 1) and nutrients were below the limit of quantitation (Fig. 6A and C). Presence of *Trichodesmium* during these environmental conditions concurs with previous observations from the Red Sea (Böttger-Schnack and Schnack, 1989; Post et al., 2002; Al-Najjar et al., 2007; Kürten et al., 2015). Typically, *Trichodesmium* is restricted to the 20–30 °C isotherms and thrives in stratified and oligotrophic seas where light intensities are high, and N concentrations are low (negative N^*) (Capone et al., 1997; Breitbarth et al., 2007). However, in our case, *Trichodesmium* did not appear as filaments at the surface in fall. The absence from the surface was either attributable to wind-induced mixing of surface waters, and/or avoidance of high UV-induced mortality (Mojib et al., 2016). Thus, both processes may help explaining the absence of *Trichodesmium* from the surface despite increased numbers in the upper layers (Fig. 8C).

Other noteworthy diazotrophs in the Red Sea are the DDAs of the diatoms *Rhizosolenia* and *Hemiaulus* (Kimor et al., 1992; Böttger-Schnack, 1995; Kürten et al., 2015). *Hemiaulus* was the most abundant diatom genus, and larger abundances of symbiont-containing *Rhizosolenia* were observed in fall. Together, *Trichodesmium* and DDAs may form a principal source of N available to higher trophic levels and

contribute significantly to macronutrient export. Yet, the quantitative contribution of N by other unicellular diazotrophs (e.g., *Crocosphaera* and relatives of *Cyanothece*) that plays a central role in the nutrient cycling in other oceans (Montoya et al., 2004; Sohm et al., 2011a; Zehr, 2011), remains subject to future investigations in the Red Sea.

A high diversity of dinoflagellates has been documented in the Red Sea, especially during stratified periods (Halim, 1969; Weikert, 1987; Ismael, 2015; Kürten et al., 2015; Devassy et al., 2017). In fall, heterotrophic dinoflagellates and microzooplankton (primarily tintinnids) were abundant. Heterotrophic dinoflagellates forage on prey from a very broad size-range, while simultaneously being prey of other dinoflagellates and zooplankton (Stoecker and McDowell Capuzzo, 1990; Jeong, 1999; Sherr and Sherr, 2007). In our study, *Podolampas palmipes*, *Protoperidinium elegans,* and *P. pellucidum* were the most prominent dinoflagellate taxa. *P. palmipes* is known to feed exclusively on bacteria with clearance rates similar to those of tintinnid microzooplankton (Lessard and Swift, 1985). *P. elegans* is a non-pigmented heterotrophic dinoflagellate (Sherr and Sherr, 2007) that feeds on bacteria as well as autotrophic cyanobacteria (*Synechococcus*) (Jeong et al., 2005). As *P. elegans* lack chlorophyll pigments, its abundance is not reflected in the chlorophyll concentration. The higher concentration of dissolved organic matter, bacteria, and biomass of Cyanobacteria (*Synechococcus*) could be a sufficient food source for dinoflagellates in the Red Sea.

The overall low productivity and plankton standing stock in fall can be influenced by the lateral advection of GAW. Recent studies indicated the presence of GAIW in the central Red Sea and characterized it by its low salinity, elevated chlorophyll and CDOM (Churchill et al., 2014; Wafar et al., 2016a; Zarokanellos et al., 2017a). In this study, the presence of GAIW in the southcentral Red Sea elevated chlorophyll fluorescence at intermediate depths and increased the integrated chlorophyll concentration at NC1-8 (Figs. 2D and 8E), but this enhancement was only weakly reflected in increased net-phytoplankton counts and not noticeable via pigment-based assessments of phytoplankton biomass and composition.

Microzooplankton was also abundant in fall. Microzooplankton typically forages on heterotrophic bacteria and picoplankton and consume > 70% of phytoplankton production in tropical/subtropical seas (Calbet and Landry, 2004). Substantial grazing on heterotrophic bacteria and picoplankton (but not *Synechococcus*) was previously observed in the Red Sea (Sommer et al., 2002a). In fall, mixo-/heterotrophic dinoflagellates and microzooplankton may form a central trophic link to suspension-feeding zooplankton and some predatory copepods, which is coherent with other studies (Stoecker and McDowell Capuzzo, 1990; Stoecker, 1999; Dolan et al., 2012). Particularly in CDOM-rich and detritus-dominated food webs like the Red Sea, the supply of essential macronutrients, and the utilization of bacterial resources are vital for higher trophic levels (Stoecker and McDowell Capuzzo, 1990). The high abundance of Protozoa and small zooplankton taxa such as *Oncaea* and *Oithona* in the Red Sea (e.g., Halim, 1969; Weikert, 1982; Böttger-Schnack, 1995; Kürten et al., 2015) may be supported by heterotrophic microbes which consume detritus and dissolved organic matter that episodically advects as GAW (Zarokanellos et al., 2017a), and sloppy-feeding of copepods on *Trichodesmium* (Hygum et al., 1997; Steinberg et al., 2004; Ducklow and Doney, 2013). Our observations are consistent with conclusions by Kürten et al. (2016) who suggested that facultative omnivory of small Copepoda (*Oncaea*, *Oithona)* plays a key role in the trophodynamics of the Red Sea where a large fraction of phytoplankton biomass (high *Synechococcus* biomass) is inaccessible to mesozooplankton.

4.2.2. Plankton community in spring

In spring 2015, weaker stratification, mesoscale eddy activity, and lateral advection of GASW increased the nutrient availability in the central Red Sea. The plankton community responded to the higher nutrient availability as indicated by increased phytoplankton and larval zooplankton numbers and biomass, particularly of diatoms, Prasinophytes and Chrysophytes (Fig. 8C–F, Supplementary Fig. 2, Supplementary Table 1). The prominence of aforementioned phytoplankton groups upon increasing nutrient availability has been related to convective mixing (northern Red Sea) as well as GAIW inflow (southern Red Sea) (Halim, 1969; Seeberg-Elverfeldt et al., 2004b; Kürten et al., 2016; Pearman et al., 2017). The larger overall abundance of autotrophs in spring reduces the predation pressure from heterotrophic dinoflagellates, and may offer an ecological advantage to other small phytoplankton (i.e. Prymnesiophytes and Prasinophytes) which contribute substantially to the phytoplankton biomass in subsurface layers of the Red Sea (Carvalho et al., 2018). Besides, also the increased *Prochlorococcus* biomass at the DCM may be attributable to mesoscale eddy activity in spring, and the increased nutrient availability from below the 28 kg m^{-3} isopycnal may help explain the niche partitioning of cyanobacterial ecotypes in the Red Sea (Shibl et al., 2014).

While this is the first study of the Red Sea to directly relate phytoplankton communities at high taxonomic resolution to physical dynamics, our data differ at species level from previous observations due to seasonal and interannual variability (c.f. (Halim, 1969; Shaikh et al., 1986; Seeberg-Elverfeldt, 2004). Although the Red Sea is ostensibly oligotrophic and dominated by picophytoplankton (Gradinger et al., 1992), diatoms contribute substantially to the macronutrient export in the Red Sea (Seeberg-Elverfeldt et al., 2004a). Among the most conspicuous diatom genera in the Red Sea are *Rhizosolenia*, *Hemiaulus*, *Chaetoceros,* and *Thalassiosira*. In our study region, particularly at NC2-3 and NC2-6, the nano-planktonic, chain-forming diatoms *Chaetoceros* and *Thalassiosira* became more numerous, which corroborates that both taxa respond to episodic nutrient availability with disproportionately large contribution to new primary production (Goldman, 1993; McGillicuddy et al., 1998; Benitez-Nelson et al., 2007; Waite et al., 2007). As chain-formers and r-strategists, these diatoms escape grazing during mixing events in the Red Sea (Sommer et al., 2002a; Al-Najjar et al., 2007), although harpacticoid zooplankton (i.e. *Macrosetella*) consume *Thalassiosira* chains (Kürten et al., 2016). Another frequently encountered diatom species in the Red Sea is *Pseudo-nitzschia cuspidata* (Al-Aidaroos et al., 2018); this study), known to deter grazers by means of domoic acid production (Olson et al., 2006; Trainer et al., 2009). Its increased presence at stations with high zooplankton abundances may indicate that toxin-producing taxa such as *P. cuspidata* may occasionally thrive in the Red Sea as it grows well under high irradiances and on a variety of N substrates (Auro and Cochlan, 2013).

Furthermore, the positive Si^* values in spring point to an ecological advantage of DDAs due to the diatoms' Si requirement and their symbionts' N_2 fixation potential (Fig. 8D). Despite free-living *Richelia* and abundant *Hemiaulus* at NC2-6, associations with symbionts were not observed. This could be an early indicator of a succession stage in which diazotrophs (*Trichodesmium*, DDAs) play an important role since free-living symbionts can re-associate with diatom hosts when P and iron become bioavailable and sustain populations of DDAs (Tuo et al., 2017). Also Chrysophytes may have benefitted from the mesoscale eddy activity and lateral advection of dissolved organic matter from the Gulf of Aden (Brewin et al., 2015; Zarokanellos et al., 2017a). Chrysophytes contributed up to ~24% and ~29% to the phytoplankton biomass at NC2-2 and NC2-5, respectively (Supplementary Fig. 2, Supplementary Table 1). As facultative heterotrophs, Chrysophytes can switch quickly from autotrophic growth to ingestion of particulate food as well as dissolved organic material (Sandgren et al., 1995). Thus, Chrysophytes may have an ecological advantage when nutrients become available episodically, for example, during periods of high eddy activity and/or via GAW inflow.

Moreover, Chrysophytes may also benefit from Si available through dust deposits (Sandgren et al., 1995). The input of aeolian dust and aerosols during the spring to summer transition period have been considered as additional sources of nutrients and trace metals for plankton in the Red Sea (Banks et al., 2017). Dust storm deposits collected in the coastal region of the central Red Sea include many

elements that are vital for primary producers, including silicon dioxide (SiO_2: ~53.8%), readily soluble phosphor (P_2O_5: ~0.24%), total nitrogen (0.7 mg g^{-1}), iron (30.4 ± 0.4 mg g^{-1}), magnesium (1.6 ± 0.1 mg g^{-1}), and manganese (0.5 ± 0.1 mg g^{-1}) (Kürten, Pollehne, and Struck, in prep.). It is not surprising that siliceous algae (i.e. diatoms, Chrysophytes) play an important role in a region where dust storms are frequent, and in turn chlorophyll anomalies occur (Rao et al., 1999; Prakash et al., 2015; Li et al., 2018). Thus, the addition of dust-associated nutrients, together with diazotrophs included in aerosols (Rahav et al., 2018), all have the potential to increase primary production and N_2 fixation in the Red Sea; but see (Torfstein and Kienast, 2018).

4.3. Resource competition in the Red Sea

Bottom–up (physical processes) and top–down processes (grazing) are joint determinants of the phytoplankton biomass (improvement of growth conditions) and species composition (predation avoidance) (Menge, 2000; Sommer et al., 2002b). The primary production in the euphotic layer of the Red Sea is controlled primarily by the availability of nutrients (Shaikh et al., 1986; Sommer, 2000). Over seasons, the composition of the phytoplankton community shifts (episodically) from a picoplankton/heterotrophic community (dinoflagellates, diazotrophs) to a diatom-dominated community when nutrients become available via eddies or advection of GAW (Halim, 1969; Kürten et al., 2016; this study). Our observation is consistent with nutrient addition experiments which highlighted the importance of resource limitation over grazing control in the Red Sea (Sommer, 2000; Sommer et al., 2002a; Rahav et al., 2015; Pearman et al., 2016b).

In oligotrophic regions such as the Red Sea, the DCM is situated in deeper layers due to the interplay between nutrient and light availability. In this study, the in situ observations show that the depths of the DCM were typically deeper than those of the Z_{Eu}. Our results confirm that nutrient limitation increases the picoplankton biomass in the Red Sea and supports the growth of diazotrophs when nutrient availability decreases. Besides, even in the absence of river runoff and rainfall in the study area, dust can be an significant alternative source of new nutrients, as primary producers as well as diazotroph communities may benefit from dust deposits (Prakash et al., 2015; Li et al., 2018). Hence, dust storms may trigger changes in the food web architecture and partially explain the heterogeneity in primary production and export in time and space.

As suggested in our previous study (Kürten et al., 2016), we confirm that bottom-up and top-down processes control the dynamic balance in the continuum between trophic pathways, i.e. the herbivorous, multivorous, and the microbial food web (Legendre and Rassoulzadegan, 1995). We show that responses to nutrient availability, on the one hand, alter the phytoplankton communities (bottom-up control) in the Red Sea, but emphasize that increased nutrient availability, on the other hand, is not always noticeable in increased integrated chlorophyll concentrations as grazing can be substantial (top-down control). It remains to be assessed, to what extent diazotrophs communities and the magnitude of C and N fixation in the Red Sea are influenced by GAW intrusions and mesoscale eddies.

4.4. Implications of food web architecture for metabolism and export

The physical dynamics of the Red Sea are key drivers of plankton distribution, production, and export (e.g., (Halim, 1969; Sicha et al., 2009); this study). The present study adds insight into the question, whether the ecosystem metabolism in the Red Sea is mostly autotrophic or heterotrophic (Ducklow and Doney, 2013). Autotrophy implies a food web architecture with substantial (often diatom-based) new production, whereas under heterotrophic conditions the regeneration-based production is dominated by picophytoplankton (e.g., *Prochlorococcus*, *Synechococcus*), mixo-/heterotrophic dinoflagellates, and microzooplankton (Sommer et al., 2002b; Ducklow and Doney, 2013; Shibl et al., 2014). Our study of plankton communities in relation to the physical dynamics indicate that mesoscale eddy activity, lateral advection of GAW, and mixing control the ecosystem metabolism in space and time.

We consider the largely herbivorous (green) food web in spring and the detritus-based (brown) microbial food web in fall as two end members of interconnected food webs (Legendre and Rassoulzadegan, 1995; Sterner and Elser, 2002). As nutrients became available in the upper layer due to mesoscale eddy activity, the abundances of diatoms and other autotrophs (Prasinophytes) increased and shifted the community toward an autotrophic state. Conversely, strongly stratified conditions in fall resulted in quantitative and stoichiometric nutrient limitation (negative N^*), and the community was dominated by *Synechococcus* and mixo-/heterotrophs. Eddies alter the configuration of the planktonic food web by episodically swinging the ecosystem metabolism from heterotrophy to autotrophy. However, the role of GAW regarding the ecosystem metabolism in the central Red Sea remains to be further assessed. Albeit increased chlorophyll concentration, GAW masses in our study were not accompanied with increased nutrient or dissolved organic matter concentrations as described by Zarokanellos et al. (2017a).

At large (geological) time scale, seasonal shifts from autotrophic to heterotrophic plankton metabolism and productivity are recorded in the sediments of the Red Sea. Particularly the species composition of diatoms in sediment layers indicate seasonal changes in stratification/mixing and the associated export from the upper water column (Seeberg-Elverfeldt et al., 2004a, 2005). The sediment lamination points to a perseverant deposition cycle for the past 15,000 years which indicate two contrasting seasons and associated plankton communities (Shaikh et al., 1986; Seeberg-Elverfeldt et al., 2004a). As described in the present study, stratified conditions in the Red Sea are characterized by assemblages of the diatom genus *Rhizosolenia*, while fast-growing *Chaetoceros* assemblages reflect deep convective mixing conditions and near-surface productivity due to upwelling (Seeberg-Elverfeldt et al., 2004a).

Moreover, in addition to macronutrient export by diatoms, also diazotrophs may contribute significantly to the vertical flux in the Red Sea as described from other oceans (Scharek et al., 1999; Benitez-Nelson et al., 2007; Sohm et al., 2011b). Since nitrogenous nutrient scarcity was associated with increased abundances of diazotrophs and diatoms with the potential for DDAs (i.e. *Rhizosolenia*, *Hemiaulus*), and *Trichodesmium* was observed even to depths of 450 m depths (Böttger-Schnack and Schnack, 1989), we suggest that *Trichodesmium* and DDAs are responsible for large fraction of macronutrient export in the Red Sea, which could help explain the variability and patchiness of nutrient concentrations observed in deeper layers of the Red Sea (Wafar et al., 2016b).

5. Conclusions

In the present study, we elucidated the underpinning processes that drive nutrient and energy fluxes in the Red Sea. We showed how physicochemical processes modulate plankton communities and ecosystem metabolism in the Red Sea. The plankton communities are under the influence of stratification, lateral advection of GAW, mesoscale eddy activity, dust deposition (bottom–up processes), and grazing (top–down) control. In the study area, the reduced nutrient availability drives the plankton community to a heterotrophic state during which regeneration production dominates. In fall, strong stratification increased the presence of heterotrophs (Fig. 9). The increased stratification reduced the nutrient availability and enhanced the abundances of diazotrophs (*Trichodesmium*, DDAs) which are able to compensate the lack of N by fixation of atmospheric N_2. With the presence of a diverse diazotroph community in the Red Sea (Mohamed, 2018), our study advocates that non-diazotrophic plankton in the Red Sea is limited

primarily by the availability of P (Figs. 6C, D and 8C, D). This view is supported by Stihl et al. (2001), who showed that *Trichodesmium* and the co-occurring *Synechococcus* populations both elevate the level of alkaline phosphatase activity in P depleted waters in the Red Sea. However, since the Red Sea region receives high dust deposits (Prakash et al., 2015), plankton communities may benefit from the availability of new P and Si and the associated changes in nutrient stoichiometry.

Our observations show a shift of the plankton community between fall 2014 and spring 2015 from a mostly heterotrophic community to an autotrophic community metabolism, respectively. In spring, plankton communities responded to the availability of new nutrients through the presence of mesoscale eddy activity and GAW. The former enhanced the biomass of autotrophs (diatoms, Prasinophytes) and supported increased numbers of zooplankton and their larval stages. These changes in ecosystem metabolism of the Red Sea are associated with a seasonal modulation of the plankton community, as indicated by *Trichodesmium* and DDAs as well as *Rhizosolenia* and *Chaetoceros* abundances. The latter may contribute significantly to the macronutrient export, while N export by *Trichodesmium* and DDAs may profoundly change the N budget of the subsurface nutrient field. The present study also showed that $\delta^{18}O_{SW}$ traced GAW in the upper layer of the central Red Sea.

Information about the relationships between physical dynamics and plankton community metabolism are key to understand the effects of global climate change scenarios for increasing temperature and anthropogenic nutrient loading. Rising temperatures of the global oceans may strengthen the stratification, reduce mesoscale eddy activity and thereby the nutrient availability from deeper layers. Under these conditions, diazotrophs that are fundamental for nutrient fluxes in the Red Sea (Naqvi et al., 1986), may play an larger role in the nutrient cycling the future. However, increasing evaporation may also enhance the thermohaline overturning circulation and alter the import of nutrient- and plankton-rich GAW. Thus, knowledge about the identity of diazotroph taxa and corresponding N_2 fixation rates in the Red Sea will be fundamental for models of biogeochemical cycles and macronutrient export.

Also, at the current state of urban run-off, nutrient inflow from metropolitan cities are less likely to influence the open Red Sea (Peña-García et al., 2014), even though mass developments of potentially harmful algae have been observed (Kürten et al., 2015; Al-Aidaroos et al., 2018). In the future, however, urban and industrial development is likely to increase nutrient availability and alter the nutrient budget of the Red Sea. It is therefore imperative that ecosystem-based management practices consider shelf-exchange processes and processes that affect the availability and composition of dust. To resolve potential nutrient fluxes and their magnitude in the Red Sea, further understanding of the physical and biogeochemical exchanges between the coastal region and the open sea is required.

Disclosure

BJ acquired project funding. BK and BJ conceived the study. BK led the research cruises. BK, RD and IS carried out field work. MS, RD and AA analyzed plankton samples. US measured water isotopes. BK and NZ evaluated the data and wrote the manuscript. BJ, DC, US, IS, and XI provided editorial remarks. All authors consented to the article.

Acknowledgements

We thank the captains and crew of R/V *Thuwal*, cruise participants, and the King Abdullah University of Science and Technology (KAUST) Coastal and Marine Resources Core Laboratories (CMOR). We are indebted to T. Gunderson, M. Tiahlo and M. Morando (USC) for providing ammonia data. We are thankful for the support from S. Kürten and P. Ruiz-Compean in the laboratory, S. Tiwari for providing HyperPro data, and S. Steinke for remote-sensing data visualization (all KAUST). This study used E.U. Copernicus Marine Service Information. Funding for the research reported in this publication was provided by the KAUST Red Sea Research Center (RSRC) under the Center Competitive Fund FCC/1/1973-05-01 and baseline research funding BAS/1/1032-01-01 assigned to BHJ. During the writing phase of this manuscript BK and NZ were supported by baseline funds of BHJ. We acknowledge the reviewer E. Raes and one anonymous reviewer for their constructive feedback which helped to greatly improve the manuscript.

Appendix A. Supplementary material

Supplementary data to this article can be found online at https://doi.org/10.1016/j.pocean.2019.02.007.

References

Abualnaja, Y., Papadopoulos, V.P., Josey, S.A., Hoteit, I., Kontoyiannis, H., Raitsos, D.E., 2015. Impacts of climate modes on air–sea heat exchange in the Red Sea. J. Clim. 28 (7), 2665–2681.

Al-Aidaroos, A.M., Devassy, R.P., El-Sherbiny, M.M., 2018. Unusual dominance of harmful microalgae *Pseudo-nitzschia delicatissima* cf. (Cleve) Heiden in the coastal waters of Jeddah, central Red Sea. Pak. J. Bot. 51 (2), 1–6.

Al-Najjar, T., Badran, M.I., Richter, C., Meyerhoefer, M., Sommer, U., 2007. Seasonal dynamics of phytoplankton in the Gulf of Aqaba, Red Sea. Hydrobiologia 579, 69–83.

Altabet, M.A., 2006. Isotopic tracers of the marine nitrogen cycle: present and past. In: Volkman, J.K. (Ed.), Marine Organic Matter: Biomarkers, Isotopes and DNA. Springer, Berlin, pp. 251–293.

Andrié, C., Merlivat, L., 1989. Contribution des données isotopiques de deutérium, oxygène-18, hélium-3 et tritium, à l'étude de la circulation de la Mer Rouge. Oceanolog. Acta 12 (3), 165–174.

Auro, M.E., Cochlan, W.P., 2013. Nitrogen Utilization and Toxin Production by Two Diatoms of the *Pseudo-nitzschia pseudodelicatissima* Complex: *P. cuspidata* and *P. fryxelliana*. J. Phycol. 49 (1), 156–169.

Azam, F., Fenchel, T., Field, J.G., Gray, J.S., Meyer-Reil, L.-A., Thingstad, F., 1983. The ecological role of water-column microbes in the sea. Mar. Ecol.-Prog. Ser. 10, 257–263.

Banks, J.R., Brindley, H.E., Stenchikov, G., Schepanski, K., 2017. Satellite retrievals of dust aerosol over the Red Sea, 2005–2015. Atmos. Chem. Phys. Discuss. 17, 3987–4003.

Barlow, E., 1934. Currents of the Red Sea and part of the Indian Ocean north of Australia. Mar. Observ. 110, 150–154.

Beckmann, W., 1984. Mesozooplankton distribution on a transect from the Gulf of Aden to the central Red Sea during the winter monsoon. Oceanol. Acta 7 (1), 87–102.

Benitez-Nelson, C.R., Bidigare, R.R., Dickey, T.D., Landry, M.R., Leonard, C.L., Brown, S.L., Nencioli, F., Rii, Y.M., Maiti, K., Becker, J.W., 2007. Mesoscale eddies drive increased silica export in the subtropical Pacific Ocean. Science 316 (5827), 1017–1021.

Bibby, T., Moore, C., 2011. Silicate: nitrate ratios of upwelled waters control the phytoplankton community sustained by mesoscale eddies in sub-tropical North Atlantic and Pacific. Biogeosciences 8 (3), 657–666.

Bigg, G.R., Rohling, E.J., 2000. An oxygen isotope data set for marine waters. J. Geophys. Res.: Oceans 105 (C4), 8527–8535.

Bonnet, S., Dekaezemacker, J., Turk-Kubo, K.A., Moutin, T., Hamersley, R.M., Grosso, O., Zehr, J.P., Capone, D.G., 2013. Aphotic N_2 fixation in the Eastern Tropical South Pacific Ocean. PLoS ONE 8 (12), e81265.

Böttger-Schnack, R., Schnack, D., 1989. Vertical distribution and population structure of *Macrosetella gracilis* (Copepoda: Harpacticoida) in the Red Sea in relation to the occurrence of *Oscillatoria (Trichodesmium*) spp (Cyanobacteria). Mar. Ecol.-Prog. Ser. 52 (1), 17–31.

Böttger-Schnack, R., 1995. Summer distribution of micro- and small meso-zooplankton in the Red Sea and Gulf of Aden, with special reference to non-calanoid copepods. Mar. Ecol.-Prog. Ser. 118, 81–102.

Bower, A.S., Farrar, J.T., 2015. Air–sea interaction and horizontal circulation in the Red Sea. In: Rasul, N.M.A., Stewart, I.C.F. (Eds.), The Red Sea. Springer, Heidelberg, pp. 329–342.

Brathwaite, C.J.R., 1987. Geology and Paleogeography of the Red Sea region. In: Edwards, A.J., Head, S.M. (Eds.), Key Environments – Red Sea. Pergamon Press, Oxford, pp. 22–44.

Breitbarth, E., Oschlies, A., LaRoche, J., 2007. Physiological constraints on the global distribution of *Trichodesmium* – Effect of temperature on diazotrophy. Biogeosciences 4 (1), 53–61.

Brewin, R.J.W., Raitsos, D.E., Dall'Olmo, G., Zarokanellos, N., Jackson, T., Racault, M.-F., Boss, E.S., Sathyendranath, S., Jones, B.H., Hoteit, I., 2015. Regional ocean-colour chlorophyll algorithms for the Red Sea. Remote Sens. Environ. 165, 64–85.

Calbet, A., Landry, M.R., 2004. Phytoplankton growth, microzooplankton grazing, and carbon cycling in marine systems. Limnol. Oceanogr. 49 (1), 51–57.

Capone, D.G., Zehr, J.P., Paerl, H.W., Bergman, T., Bergman, B., Carpenter, E.J., 1997. *Trichodesmium*, a globally significant marine cyanobacterium. Science 276 (5316), 1221–1229.

Carvalho, S., Kürten, B., Krokos, G., Hoteit, I., Ellis, J., 2018. The Red Sea. In: Sheppard, C. (Ed.), World Seas: An Environmental Evaluation. Volume II: The Indian Ocean to the Pacific, second ed. Academic Press, London, pp. 49–74.

Chen, C., Li, R., Pratt, L., Limeburner, R., Beardsley, R.C., Bower, A., Jiang, H., Abualnaja, Y., Xu, Q., Lin, H., 2014. Process modeling studies of physical mechanisms of the formation of an anticyclonic eddy in the central Red Sea. J. Geophys. Res. [Oceans] 119 (2), 1445–1464.
Churchill, J.H., Bower, A.S., McCorkle, D.C., Abualnaja, Y., 2014. The transport of nutrient-rich Indian Ocean water through the Red Sea and into coastal reef systems. J. Mar. Res. 72 (3), 165–181.
Craig, H., Gordon, L.I., 1965. Deuterium and oxygen 18 variations in the ocean and the marine atmosphere. In: Tongiorgi, E. (Ed.), Stable Isotopes in Oceanographic Studies and Paleotemperatures. Cons Naz. di Rech, pp. 9–130.
Craig, H., 1966. Isotopic composition and origin of the Red Sea and Salton Sea geothermal brines. Science 154 (3756), 1544–1548.
de Boyer Montégut, C., Madec, G., Fischer, A.S., Lazar, A., Iudicone, D., 2004. Mixed layer depth over the global ocean: an examination of profile data and a profile-based climatology. J. Geophys. Res. [Oceans] 109, (C12003).
Deutsch, C., Weber, T., 2012. Nutrient ratios as a tracer and driver of ocean biogeochemistry. Annu. Rev. Mar. Sci. 4, 113–141.
Devassy, R.P., El-Sherbiny, M.M., Al-Sofyani, A.M., Al-Aidaroos, A.M., 2017. Spatial variation in the phytoplankton standing stock and diversity in relation to the prevailing environmental conditions along the Saudi Arabian coast of the northern Red Sea. Mar. Biodivers. 1–14.
Dolan, J.R., Montagnes, D.J.S., Agatha, S., Coats, D.W., Stoecker, D.K., 2012. The Biology and Ecology of Tintinnid Ciliates: Models for Marine Plankton. John Wiley & Sons Ltd, Chichester, pp. 1–319.
Dreano, D., Raitsos, D.E., Gittings, J., Krokos, G., Hoteit, I., 2016. The Gulf of Aden intermediate water intrusion regulates the southern red sea summer phytoplankton blooms. PLoS ONE 11 (12), e0168440.
Ducklow, H.W., Doney, S.C., 2013. What is the metabolic state of the oligotrophic ocean? A debate. Annu. Rev. Mar. Sci. 5, 525–533.
Egge, J., Aksnes, D., 1992. Silicate as regulating nutrient in phytoplankton competition. Mar. Ecol.-Prog. Ser. 83, 281–289.
Ehrenberg, C.G., 1830. Neue Beobachlungen über blutartige Erscheinungen in Aegypten, Arabien und Sibirien, nebst einer Uebersicht und Kritik der früher bekannnten. Annalen der Physik 94 (4), 477–514.
Foster, R.A., Paytan, A., Zehr, J.P., 2009. Seasonality of N_2 fixation and *nifH* gene diversity in the Gulf of Aqaba (Red Sea). Limnol. Oceanogr. 54 (1), 219–233.
Ganssen, G., Kroon, D., 1991. Evidence for Red Sea surface circulation from oxygen isotopes of modern surface waters and planktonic foraminiferal tests. Paleoceanography 6 (1), 73–82.
Goldman, J.C., 1988. Spatial and Temporal Discontinuities of Biological Processes in Pelagic Surface Waters. In: Rothschild, B.J. (Ed.), Toward a Theory on Biological-Physical Interactions in the World Ocean. Springer, Netherlands, Dordrecht, pp. 273–296.
Goldman, J.C., 1993. Potential role of large oceanic diatoms in new primary production. Deep Sea Res. Part I 40 (1), 159–168.
Gradinger, R., Weisse, T., Pillen, T., 1992. Significance of picocyanobacteria in the Red Sea and the Gulf of Aden. Bot. Mar. 35, 245–250.
Grasshoff, K., 1969. Zur Chemie des Roten Meeres und des Inneren Golfs von Aden nach Beobachtungen von FS "Meteor" während der Indischen Ozean Expedition 1964/65. Meteor Forschungsergebnisse, Deutsche Forschungsgemeinschaft, Reihe A Allgemeines, Physik und Chemie des Meeres. Gebrüder Bornträger, Berlin, Stuttgart, pp. 1–76.
Halim, Y., 1969. Plankton of the Red Sea. Oceanogr. Mar. Biol. Annu. Rev. 7, 231–275.
Hauss, H., Franz, J.M.S., Hansen, T., Struck, U., Sommer, U., 2013. Relative inputs of upwelled and atmospheric nitrogen to the eastern tropical North Atlantic food web: Spatial distribution of $\delta^{15}N$ in mesozooplankton and relation to dissolved nutrient dynamics. Deep Sea Res. Part I 75, 135–145.
Hemleben, C., Meischner, D., Zahn, R., Almogi-Labin, A., 1996. Three hundred eighty thousand year long stable isotope and faunal records from the Red Sea: Influence of global sea level change on hydrography. Paleoceanography 11 (2), 147–156.
Holmes, R.M., Aminot, A., Kérouel, R., Hooker, B.A., Peterson, B.J., 1999. A simple and precise method for measuring ammonium in marine and freshwater ecosystems. Canad. J. Fish. Aquat Sci. 56 (10), 1801–1808.
Horita, J., Ueda, A., Mizukami, K., Takatori, I., 1989. Automatic δD and $\delta^{18}O$ analyses of multi-water samples using H_2- and CO_2-water equilibration methods with a common equilibration set-up. Int. J. Rad. Appl. Instrum. [A] 40 (9), 801–805.
Hygum, B.H., Petersen, J.W., Søndergaard, M., 1997. Dissolved organic carbon released by zooplankton grazing activity-a high-quality substrate pool for bacteria. J. Plankton Res. 19 (1), 97–111.
IOC, SCOR, IAPSO, 2010. The international thermodynamic equation of seawater – 2010: Calculation and use of thermodynamic properties. In: IO Commission (Ed.), Manuals and Guides. United Nations Educational, Scientific and Cultural Organization, Paris, pp. 1–196.
Ismael, A.A., 2015. Phytoplankton of the Red Sea. In: Rasul, N.M.A., Stewart, I.C.F. (Eds.), The Red Sea: The Formation, Morphology, Oceanography and Environment of a Young Ocean Basin. Springer, Heidelberg, pp. 567–583.
Jeong, H.J., 1999. The ecological roles of heterotrophic dinoflagellates in marine planktonic community. J. Eukaryot. Microbiol. 46 (4), 390–396.
Jeong, H.J., Park, J.Y., Nhi, J.H., Park, M.O., Ha, J.H., Seong, K.A., Cheng, C., Seong, C.N., Lee, Q.Y., Yih, W.H., 2005. Feeding by red-tide dinoflagellates on the cyanobacterium *Synechococcus*. Aquat Microb. Ecol. 41, 131–143.
Johns, W.E., Sofianos, S.S., 2012. Atmospherically forced exchange through the Bab el Mandeb Strait. J. Phys. Oceanogr. 42 (7), 1143–1157.
Jones, E.N., Browning, D.G., 1971. Cold water layer in the southern Red Sea. Limnol. Oceanogr. 16 (3), 503–509.
Kheiredine, M., Ouhssain, M., Claustre, H., Uitz, J., Gentili, B., Jones, B.H., 2017. Assessing pigment-based phytoplankton community distributions in the Red Sea. Front. Mar. Sci. 4 (132).
Kimor, B., Gordon, N., Neori, A., 1992. Symbiotic associations among microplankton in oligotrophic marine environments, with special reference to the Gulf of Aqaba. Red Sea. J. Plankton Res. 14 (9), 1217–1231.
Kürten, B., Al-Aidaroos, A.M., Struck, U., Khomayis, H.S., Gharbawi, W.Y., Sommer, U., 2014. Influence of environmental gradients on C and N stable isotope ratios in coral reef biota of the Red Sea. Saudi Arabia. J. Sea Res. 85, 379–394.
Kürten, B., Khomayis, H.S., Devassy, R., Audritz, S., Sommer, U., Struck, U., El-Sherbiny, M.M., Al-Aidaroos, A.M., 2015. Ecohydrographic constraints on biodiversity and distribution of phytoplankton and zooplankton in coral reefs of the Red Sea, Saudi Arabia. Mar. Ecol. 36 (4), 1195–1214.
Kürten, B., Al-Aidaroos, A.M., Kürten, S., El-Sherbiny, M.M., Devassy, R.P., Struck, U., Zarokanellos, N., Jones, B.H., Hansen, T., Bruss, G., Sommer, U., 2016. Carbon and nitrogen stable isotope ratios of pelagic zooplankton elucidate ecohydrographic features in the oligotrophic Red Sea. Prog. Oceanogr. 140, 69–90.
Legendre, L., Rassoulzadegan, F., 1995. Plankton and nutrient dynamics in marine waters. Ophelia 41, 153–172.
LeGresley, M., McDermott, G., 2010. Counting chamber methods for quantitative phytoplankton analysis—haemocytometer, Palmer-Maloney cell and Sedgewick-Rafter cell. In: Karlson, B., Cusack, C., Bresnan, E. (Eds.), Microscopic and Molecular Methods for Quantitative Phytoplankton Analysis. United Nations Educational Scientific and Cultural Organization, Paris, pp. 25–30.
Lessard, E.J., Swift, E., 1985. Species-specific grazing rates of heterotrophic dinoflagellates in oceanic waters, measured with a dual-label radioisotope technique. Mar. Biol. 87 (3), 289–296.
Li, W., El-Askary, H., Qurban, M.A., Proestakis, E., Garay, M.J., Kalishnikova, O.V., Amiridis, V., Gkikas, A., Marinou, E., Piechota, T., 2018. An assessment of atmospheric and meteorological factors regulating red sea phytoplankton growth. Remote Sens. 10 (5).
Lindell, D., Post, A.F., 1995. Ultraphytoplankton succession is triggered by deep winter mixing in the Gulf of Aqaba (Eilat). Red Sea. Limnol. Oceanogr. 40 (6), 1130–1141.
Litvin, V.M., 1984. The Morphostructure of the Atlantic Ocean Floor, its Development in the Meso-Cenozoic. D. Reidel Publishing Company, Dordrecht, pp. 1–187.
McGillicuddy Jr, D.J., 2016. Mechanisms of physical-biological-biogeochemical interaction at the oceanic mesoscale. Annu. Rev. Mar. Sci. 8, 125–159.
McGillicuddy Jr., D.J., Robinson, A.R., Siegel, D.A., Jannasch, H.W., Johnson, R., Dickey, T.D., McNeil, J., Michaels, A.F., Knap, A.H., 1998. Influence of mesoscale eddies on new production in the Sargasso Sea. Nature 394, 263–266.
McGuire, K., McDonnell, J., 2007. Stable isotope tracers in watershed hydrology. In: Lajtha, K., Michener, R.H. (Eds.), Stable Isotopes in Ecology and Environmental Science. Blackwell Scientific Publications, London, pp. 334–374.
Menge, B.A., 2000. Top-down and bottom-up community regulation in marine rocky intertidal habitats. J. Exp. Mar. Biol. Ecol. 250, 257–289.
Mohamed, R., 2018. Molecular fingerprinting to understand diazotrophic microbe distribution in oligotrophic oceans. Ph.D. thesis. King Abdullah University of Science and Technology (KAUST), Thuwal, Saudi Arabia, pp. 1–170.
Mojib, N., Thimma, M., Kumaran, M., Sougrat, R., Irigoien, X., 2016. Comparative metatranscriptomics reveals decline of a neustonic planktonic population. Limnol. Oceanogr. 62 (1), 299–310.
Montoya, J.P., Holl, C.M., Zehr, J.P., Hansen, A., Villareal, T.A., Capone, D.G., 2004. High rates of N_2 fixation by unicellular diazotrophs in the oligotrophic Pacific Ocean. Nature 430 (7003), 1027–1031.
Moore, L.R., Post, A.F., Rocap, G., Chisholm, S.W., 2002. Utilization of different nitrogen sources by the marine cyanobacteria *Prochlorococcus* and *Synechococcus*. Limnol. Oceanogr. 47 (4), 989–996.
Morcos, S.A., 1970. Physical and chemical oceanography of the Red Sea. Oceanogr. Mar. Biol. Annu. Rev 8, 73–202.
Murray, S.P., Johns, W., 1997. Direct observations of seasonal exchange through the Bab el Mandab Strait. Geophys. Res. Lett. 24 (21), 2557–2560.
Naqvi, S.W.A., Hansen, H.P., Kureishy, T.W., 1986. Nutrient uptake and regeneration ratios in the Red Sea with reference to the nutrient budgets. Oceanol. Acta 9 (3), 271–275.
Neumann, A.C., McGill, D.A., 1962. Circulation of the Red Sea in early summer. Deep-Sea Res. 8, 223–235.
Officer, C., Ryther, J., 1980. The possible importance of silicon in marine eutrophication. Mar. Ecol.-Prog. Ser. 3 (1), 83–91.
Olson, M.B., Lessard, E.J., Wong, C.H.J., Bernhardt, M.J., 2006. Copepod feeding selectivity on microplankton, including the toxigenic diatoms *Pseudo-nitzschia* spp., in the coastal Pacific Northwest. Mar. Ecol.-Prog. Ser. 326, 207–220.
Painter, S.C., Sanders, R., Poulton, A.J., Woodward, E.M.S., Lucas, M., Chamberlain, K., 2007. Nitrate uptake at photic zone depths is not important for export in the subtropical ocean. Global Biogeochem. Cycl. 21 (4).
Patzert, W.C., 1974. Wind-induced reversal in Red Sea circulation. Deep Sea Res. 21, 109–121.
Pearman, J., Kürten, S., Sarma, Y., Jones, B., Carvalho, S., 2016a. Biodiversity patterns of plankton assemblages at the extremes of the Red Sea. FEMS Microbiol. Ecol. 92 (3), fiw002.
Pearman, J.K., Casas, L., Merle, T., Michell, C., Irigoien, X., 2016b. Bacterial and protist community changes during a phytoplankton bloom. Limnol. Oceanogr. 61 (1), 198–213.
Pearman, J.K., Ellis, J., Irigoien, X., Sarma, Y., Jones, B.H., Carvalho, S., 2017. Microbial planktonic communities in the Red Sea: high levels of spatial and temporal variability shaped by nutrient availability and turbulence. Sci. Rep. 7 (1), 6611.
Peña-García, D., Ladwig, N., Turki, A., Mudarris, M.S., 2014. Input and dispersion of nutrients from the Jeddah Metropolitan Area. Red Sea. Mar. Pollut. Bull. 80 (1–2),

41–51.
Post, A.F., Dedej, Z., Gottlieb, R., Li, H., Thomas, D.N., El-Absawi, M., El-Naggar, A., El-Gharabawi, M., Sommer, U., 2002. Spatial and temporal distribution of *Trichodesmium* spp. in the stratified Gulf of Aqaba, Red Sea. Mar. Ecol.-Prog. Ser. 239, 241–250.
Prakash, P.J., Stenchikov, G., Kalenderski, S., Osipov, S., Bangalath, H., 2015. The impact of dust storms on the Arabian Peninsula and the Red Sea. Atmos. Chem. Phys. 15, 199–222.
Quadfasel, D., Baudner, H., 1993. Gyre-scale circulation cells in the Red Sea. Oceanol. Acta. 16 (3), 221–229.
Qurban, M.A., Wafar, M., Jyothibabu, R., Manikandan, K., 2017. Patterns of primary production in the Red Sea. J. Mar. Sys. 169, 87–98.
Rahav, E., Herut, B., Mulholland, M.R., Belkin, N., Elifantz, H., Berman-Frank, I., 2015. Heterotrophic and autotrophic contribution to dinitrogen fixation in the Gulf of Aqaba. Mar. Ecol.-Prog. Ser. 522, 67–77.
Rahav, E., Paytan, A., Mescioglu, E., Galletti, Y., Rosenfeld, S., Raveh, O., Santinelli, C., Ho, T.Y., Herut, B., 2018. Airborne microbes contribute to N_2 fixation in surface water of the Northern Red Sea. Geophys. Res. Lett. 45, 6186–6194.
Raitsos, D.E., Pradhan, Y., Brewin, R.J.W., Stenchikov, G., Hoteit, I., 2013. Remote sensing the phytoplankton seasonal succession of the Red Sea. PLoS ONE 8 (6), e64909.
Raitsos, D.E., Yi, X., Platt, T., Racault, M.F., Brewin, R.J.W., Pradhan, Y., Papadopoulos, V.P., Sathyendranath, S., Hoteit, I., 2015. Monsoon oscillations regulate fertility of the Red Sea. Geophys. Res. Lett. 42 (3), 855–862.
Rao, V.D.S., Al-Yamani, F., Rao, V.C.N., 1999. Eolian dust affects phytoplankton in the waters off Kuwait, the Arabian Gulf. Naturwissenschaften 86 (11), 525–529.
Redfield, A.C., Ketchum, B.H., Richards, F.A., 1963. The influence of organisms on the composition of seawater. In: Hill, M.N. (Ed.), The Sea, Ideas and Observations on Progress in the Study of Seas. Interscience, New York, pp. 26–77.
Roesler, C., Uitz, J., Claustre, H., Boss, E., Xing, X., Organelli, E., Briggs, N., Bricaud, A., Schmechtig, C., Poteau, A., 2017. Recommendations for obtaining unbiased chlorophyll estimates from in situ chlorophyll fluorometers: a global analysis of WET Labs ECO sensors. Limnol. Oceanogr. Methods 15 (6), 572–585.
Rohling, E.J., Bigg, G.R., 1998. Paleosalinity and $\delta^{18}O$: A critical assessment. J. Geophys. Res. [Oceans] 103 (C1), 1307–1318.
Sandgren, C.D., Smol, J.P., Kristiansen, J., 1995. Chrysophyte Algae: Ecology, Phylogeny and Development. Cambridge University Press, Cambridge.
Sarmiento, J.L., Gruber, N., Brzezinski, M., Dunne, J., 2004. High-latitude controls of thermocline nutrients and low latitude biological productivity. Nature 427 (6969), 56–60.
Scharek, R., Tupas, L.M., Karl, D.M., 1999. Diatom fluxes to the deep sea in the oligotrophic North Pacific gyre at Station ALOHA. Mar. Ecol.-Prog. Ser. 182, 55–67.
Schmidt, G.A., Bigg, G.R., Rohling, E.J., 1999. Global Seawater Oxygen-18 Database – v1.21. https://data.giss.nasa.gov/o18data.
Seeberg-Elverfeldt, I.A., 2004. Laminated diatomaceous sediments of the Red Sea, their composition and significance as recorders of abrupt changes in productivity and circulation during the Late Quaternary. Ph.D. thesis. Bremen University, Bremen, Germany, pp. 1–127.
Seeberg-Elverfeldt, I.A., Lange, C., Pätzold, J., Kuhn, G., 2005. Laminae type and possible mechanisms for the formation of laminated sediments in the Shaban Deep, northern Red Sea. Ocean Sci. 1 (4), 113–126.
Seeberg-Elverfeldt, I.A., Lange, C.B., Arz, H.W., Pätzold, J., Pike, J., 2004a. The significance of diatoms in the formation of laminated sediments of the Shaban Deep. Northern Red Sea. Mar. Geol. 209 (1), 279–301.
Seeberg-Elverfeldt, I.A., Lange, C.B., Pätzold, J., 2004b. Preservation of siliceous microplankton in surface sediments of the northern Red Sea. Mar. Micropaleontol. 51, 193–211.
Seth, B., Schneider, C., Storck, F., 2006. Improved reliability of oxygen isotopic analysis of water using the Finnigan GasBench II periphery of a continuous flow isotope ratio mass spectrometer by backflushing of the sampling line. Rapid Commun. Mass Spectrom. 20 (6), 1049–1051.
Shaikh, E.A., Roff, J.C., Dowidar, N.M., 1986. Phytoplankton ecology and production in the Red Sea off Jiddah, Saudi Arabia. Mar. Biol. 92, 405–416.
Sherr, E.B., Sherr, B.F., 2007. Heterotrophic dinoflagellates: a significant component of microzooplankton biomass and major grazers of diatoms in the sea. Mar. Ecol.-Prog. Ser. 352, 187–197.
Shibl, A.A., Thompson, L.R., Ngugi, D.K., Stingl, U., 2014. Distribution and diversity of *Prochlorococcus* ecotypes in the Red Sea. FEMS Microbiol. Lett. 356 (1), 118–126.
Siccha, M., Trommer, G., Schulz, H., Christoph, H., Kucera, M., 2009. Factors controlling the distribution of planktonic foraminifera in the Red Sea and implications for the development of transfer functions. Mar. Micropaleontol. 72, 146–156.
Siedler, G., 1968. Schichtungs-und Bewegungsverhältnisse am Südausgang des Roten Meeres. Meteor Forschungsergebnisse, Gebrueder Borntraeger, Berlin, Reihe A, Heft 4, pp. 1–76.
Sofianos, S.S., Johns, W.E., Murray, S.P., 2002. Heat and freshwater budgets in the Red Sea from direct observations at Bab el Mandeb. Deep Sea Res. Part 2. Top. Stud. Oceanogr. 49 (7), 1323–1340.
Sofianos, S.S., Johns, W.E., 2002. An oceanic general circulation model (OGCM) investigation of the Red Sea circulation, 1. Exchange between the Red Sea and the Indian Ocean. J. Geophys. Res. [Oceans] 107, (C11).
Sofianos, S.S., Johns, W.E., 2007. Observation of the summer Red Sea circulation. J. Geophys. Res. 112, 1–20.
Sohm, J.A., Subramaniam, A., Gunderson, T.E., Carpenter, E.J., Capone, D.G., 2011a. Nitrogen fixation by *Trichodesmium* spp. and unicellular diazotrophs in the North Pacific Subtropical Gyre. J. Geophys. Res. Biogeosci. 116 (G3).
Sohm, J.A., Webb, E.A., Capone, D.G., 2011b. Emerging patterns of marine nitrogen fixation. Nat. Rev. Microbiol. 9 (7), 499–508.
Sommer, U., 2000. Scarcity of medium-sized phytoplankton in the northern Red Sea explained by strong bottom-up and weak top-down control. Mar. Ecol.-Prog. Ser. 197, 19–25.
Sommer, U., Berninger, U.-G., Böttger-Schnack, R., Cornils, A., Hagen, W., Hansen, T., Al-Najjar, T., Post, A.F., Schnack-Schiel, S.B., Stibor, H., Stübing, D., Whickham, S., 2002a. Grazing during early spring in the Gulf of Aqaba and the northern Red Sea. Mar. Ecol.-Prog. Ser. 239, 251–261.
Sommer, U., Stibor, H., Katechakis, A., Sommer, F., Hansen, T., 2002b. Pelagic food web configurations at different levels of nutrient richness and their implications for the ratio fish production:primary production. Hydrobiologia 484, 11–20.
Souvermezoglou, E., Metzl, N., Poisson, A., 1989. Red Sea budgets of salinity, nutrients and carbon calculated in the Strait of Bab-El-Mandab during the summer and winter seasons. J. Mar. Res. 47 (2), 441–456.
Steinberg, D.K., Nelson, N.B., Carlson, C.A., Prusak, A., 2004. Production of chromophoric dissolved organic matter (CDOM) in the open ocean by zooplankton and the colonial cyanobacterium *Trichodesmium* spp. Mar. Ecol.-Prog. Ser. 267, 45–56.
Sterner, R.W., Elser, J.J. (Eds.), 2002. Ecological Stoichiometry − The Biology of Elements from Molecules to Biosphere. Princeton Paperbacks, Princeton, New Jersey, pp. 1–463.
Stihl, A., Sommer, U., Post, A.F., 2001. Alkaline phosphatase activities among populations of the colony-forming diazotrophic cyanobacterium *Trichodesmium* spp. (cyanobacteria) in the Red Sea. J. Phycol. 37 (2), 310–317.
Stoecker, D.K., McDowell Capuzzo, J., 1990. Predation on Protozoa: its importance to zooplankton. J. Plankton Res. 12 (5), 891–908.
Stoecker, D.K., 1999. Mixotrophy among dinoflagellates. J. Eukaryot. Microbiol. 46 (4), 397–401.
Sverdrup, H.U., Johnson, M.W., Fleming, R.H., 1942. The Oceans: Their physics, chemistry, and general biology. Prentice-Hall, New York.
Taylor, B.W., Keep, C.F., Hall Jr, R.O., Koch, B.J., Tronstad, L.M., Flecker, A.S., Ulseth, A.J., 2007. Improving the fluorometric ammonium method: matrix effects, background fluorescence, and standard additions. J. N. Am. Benthol. Soc. 26 (2), 167–177.
Torfstein, A., Kienast, S., 2018. No correlation between atmospheric dust and surface ocean chlorophyll-a in the oligotrophic Gulf of Aqaba, Northern Red Sea. J. Geophys. Res. Biogeosci. 123 (2), 391–405.
Trainer, V.L., Wells, M.L., Cochlan, W.P., Trick, C.G., Bill, B.D., Baugh, K.A., Beall, B.F., Herndon, J., Lundholm, N., 2009. An ecological study of a massive bloom of toxigenic *Pseudo-nitzschia cuspidata* off the Washington State coast. Limnol. Oceanogr. 54 (5), 1461–1474.
Tuo, S.H., Lee Chen, Y.L., Chen, H.Y., Chen, T.Y., 2017. Free-living heterocystous cyanobacteria in the tropical marginal seas of the western North Pacific. J. Plankton Res. 39 (3), 404–422.
Villareal, T.A., Brown, C.G., Brzezinski, M.A., Krause, J.W., Wilson, C., 2012. Summer diatom blooms in the North Pacific subtropical gyre: 2008–2009. PLoS ONE 7 (4).
Wafar, M., Ashraf, M., Manikandan, K.P., Qurban, M.A., Kattan, Y., 2016a. Propagation of Gulf of Aden Intermediate Water (GAIW) in the Red Sea during autumn and its importance to biological production. J. Mar. Syst. 154 (Part B), 243–251.
Wafar, M., Qurban, M.A., Ashraf, M., Manikandan, K.P., Flandez, A.V., Balala, A.C., 2016b. Patterns of distribution of inorganic nutrients in Red Sea and their implications to primary production. J. Mar. Syst. 156, 86–98.
Waite, A.M., Muhling, B.A., Holl, C.M., Beckley, L.E., Montoya, J.P., Strzelecki, J., Thompson, P.A., Pesant, S., 2007. Food web structure in two counter-rotating eddies based on $\delta^{15}N$ and $\delta^{13}C$ isotopic analyses. Deep Sea Res. Part II 54 (8–10), 1055–1075.
Wankel, S.D., Chen, Y., Kendall, C., Post, A.F., Paytan, A., 2010. Sources of aerosol nitrate to the Gulf of Aqaba: Evidence from $\delta^{15}N$ and $\delta^{18}O$ of nitrate and trace metal chemistry. Mar. Chem. 120, 90–99.
Wasmund, N., 2017. The Diatom/Dinoflagellate Index as an indicator of ecosystem changes in the Baltic Sea. 2. Historical data for use in determination of good environmental status. Front. Mar. Sci. 4, 153.
Wedyan, M.A., Fandi, K.G., Al-Rousan, S., 2007. Bioavailability of atmospheric dissolved organic nitrogen in the marine aerosol over the Gulf of Aqaba. Aust. J. Basic Appl. Sci. 1 (3), 20–212.
Weikert, H., 1982. The vertical distribution of zooplankton in relation to habitat zones in the area of the Atlantis II deep, central Red Sea. Mar. Ecol.-Prog. Ser. 8, 129–143.
Weikert, H., 1987. Plankton and the pelagic environment. In: Edwards, A.J., Head, S.M. (Eds.), Key Environments: Red Sea. Pergamon Press, Oxford, pp. 90–111.
Welti, N., Striebel, M., Ulseth, A.J., Cross, W.F., DeVilbiss, S., Glibert, P.M., Guo, L., Hirst, A.G., Hood, J., Kominoski, J.S., MacNeill, K.L., Mehring, A.S., Welter, J.R., Hillebrand, H., 2017. Bridging food webs, ecosystem metabolism, and biogeochemistry using ecological stoichiometry theory. Front. Microbiol. 8 (1298).
Wilby, R.L., Clifford, N.J., Luca, P.D., Harrigan, S., Hillier, J.K., Hodgkins, R., Johnson, M.F., Matthews, T.K., Murphy, C., Noone, S.J., 2017. The 'dirty dozen' of freshwater science: detecting then reconciling hydrological data biases and errors. Wiley Interdisciplinary Reviews: Water.
Wyatt, T., 2014. Margalef's mandala and phytoplankton bloom strategies. Deep Sea Res. Part II 101, 32–49.
Yao, F., Hoteit, I., Pratt, L.J., Bower, A.S., Zhai, P., Köhl, A., Gopalakrishnan, G., 2014. Seasonal overturning circulation in the Red Sea: 1. Model validation and summer circulation. J. Geophys. Res. [Oceans] 119 (4), 2238–2262.
Zarokanellos, N.D., Kürten, B., Churchill, J.H., Roder, C., Voolstra, C.R., Abualnaja, Y., Jones, B.H., 2017a. Physical mechanisms routing nutrients in the Central Red Sea. J.

Geophys. Res. [Oceans] 122 (11), 9032–9046.
Zarokanellos, N.D., Papadopoulos, V.P., Sofianos, S.S., Jones, B.H., 2017b. Physical and biological characteristics of the winter-summer transition in the Central Red Sea. J. Geophys. Res. [Oceans] 122 (8), 6355–6370.
Zarokanellos, N.D., Jones, B.H., 2018. Winter mixing, mesoscale eddies and eastern boundary current: Engines for biogeochemical variability of the central Red Sea during winter/early spring period. Biogeosci. Discuss. 2018, 1–44.
Zehr, J.P., 2011. Nitrogen fixation by marine cyanobacteria. Trends Microbiol. 19 (4), 162–173.
Zhan, P., Subramanian, A.C., Yao, F., Hoteit, I., 2014. Eddies in the Red Sea: A statistical and dynamical study. J. Geophys. Res. [Oceans] 119 (6), 3909–3925.